https://doi.org/10.5194/egusphere-2024-373
Preprint. Discussion started: 28 February 2024

Assimilating Multi-site Eddy-Covariance Data to Calibrate the CH_4 Wetland Emission Module in a Terrestrial Ecosystem Model

Jalisha Theanutti Kallingal[1], Marko Scholze[1], Paul Anthony Miller[1], Johan Lindström[2], Janne Rinne[3], Mika Aurela[4], Patrik Vestin[1], and Per Weslien[5]

[1]Department of Physical Geography and Ecosystem Science, Lund University, Lund, Sweden, S-223 62
[2]Centre for Mathematical Sciences, Lund University, Lund, Sweden, S-223 62
[3]Natural Resources Institute Finland, Helsinki, Finland, FI-00 790
[4]Finnish Meteorological Institute, Helsinki, Finland, FI-00101
[5]Department of Geosciences, University of Gothenburg, Sweden, S-413 90

Correspondence: Jalisha T. Kallingal (jalisha.theanutti@nateko.lu.se)

Abstract. In this study, we use a data assimilation framework based on the Adaptive Markov Chain Monte Carlo (MCMC) algorithm to constrain process parameters in LPJ-GUESS using CH_4 eddy covariance flux observations from 14 different natural boreal and temperate wetlands. The objective is to derive a single set of calibrated parameter values. These parameters are then used in the model to validate its CH_4 flux output against 5 different types of natural wetlands situated in different locations, assessing their generality for simulating CH_4 fluxes from different boreal and temperate wetlands. The results show that the MCMC framework has substantially reduced the cost function (measuring the misfit between simulated and observed CH_4 fluxes) and facilitated detailed characterisation of the posterior distribution. A reduction of around 95 % in the cost function and approximately 50 % in RMSE were observed. The validation experiment results indicate that four out of 5 sites successfully reduced RMSE, demonstrating the effectiveness of the framework for estimating CH_4 emissions from wetlands not included in the study.

1 Introduction

Methane (CH_4) emissions from wetlands contribute 20-30 % to the total global emissions (IPCC AR6 chapter 5: Canadell et al. (2022), Saunois et al. (2020)). About one-third to one-half of these wetland emissions are from wetlands located at northern latitudes of North America, Europe and Russia (Saunois et al., 2016a). According to the IPCC AR6 report, wetlands are the largest single source of uncertainty to the global CH_4 budget estimate. It is expected to have increased uncertainties in wetland CH_4 emissions in the future (Christensen et al., 2007), partly due to climate change and partly due to spatio-temporal changes in wetland extent (that in itself is partly a consequence of climate change) (Saunois et al. (2016b), Zhang et al. (2017)). A key question to consider here is the extent to which these changes in emissions are occurring and how they will impact the future global greenhouse gas (GHG) budget and hence the climate. While current in-situ measurement techniques such as eddy-covariance (EC) observations are promising for drawing assumptions on this issue at local scales, studies to date have faced difficulties in estimating wetland CH_4 emissions over large landscapes (Saunois et al., 2020).

https://doi.org/10.5194/egusphere-2024-373
Preprint. Discussion started: 28 February 2024

An attempt to overcome this limitation through process-based modelling of global CH_4 emissions was first initiated by Fung et al. (1991) followed by Christensen and Cox (1995) and more mechanistically by Cao et al. (1996), and Walter and Heimann (2000). These models were simple in structure, and later more attention was given to model process improvement through the studies of mainly Segers and Leffelaar (2001), Gedney et al. (2004), and Zhuang et al. (2006). In the last decade more detailed models with more complexity and a wider range of applications were developed by Wania et al. (2010), Ringeval et al. (2010), Susiluoto et al. (2018) etc. All of these past efforts indicate that comprehensive, process-based modelling of CH_4 emissions from wetland ecosystems is unquestionably a key way to understand the variability of wetlands and how they respond to stresses and climate change (Saunois et al., 2020).

As all these models are approximations of the real world and exhibit their own uncertainties, here again the question is how to reduce the uncertainty for large-scale applications. According to Kuppel et al. (2012) every terrestrial biosphere model contains uncertainties in 5 different ways: errors in real data used for calibration, errors in meteorological forcing, errors in process descriptions, errors in model parameter values, and inaccurate initial state of the model. The first two errors are related to measurement, while the last three are related to model formulation and are important to improve the model performance for general applications. There has been a growing effort to reduce uncertainty related to the last three sources of error factors in several ways. A popular method to reduce uncertainty in model parameters is to calibrate the model simulations against observations. Previous studies like Williams et al. (2009), Susiluoto et al. (2018) and Kuppel et al. (2012), based on different models, different data and different parameter sets provide examples of improving model parameters and reducing uncertainties through data assimilation.

In this study, we consider uncertainties in parameter values of the CH_4 module of a global process-based ecosystem model, Lund–Potsdam–Jena General Ecosystem Simulator (LPJ-GUESS) v4.1 and aim to reduce their uncertainties by assimilating EC CH_4 flux observations collected at 14 different arctic, boreal and temperate wetland sites. Dynamic Global Vegetation Models (DGVMs) like LPJ-GUESS are state-of-the-art tools for studying the functioning of high-latitude wetlands and estimating the dynamics in their global carbon balance (Sitch et al., 2003). In a previous study, Kallingal et al. (2023) have used EC data collected at an individual site to investigate the potential of a Markov Chain Monte Carlo (MCMC) type (Global Rao-Black-wellised Adaptive Metropolis, GRaB-AM) algorithm to optimise the parameters in the CH_4 module of LPJ-GUESS. The study showed that eddy covariance measurements of CH_4 flux contain useful information for optimising the CH_4 model parameters due to the high temporal resolution of the CH_4 flux measurements. However, the small spatial scale (site scale) and limited temporal extent of data collected from a single site could have over fitted parameters to the specificities of the particular site used. This points to the need for a more general approach. For example, in a study conducted by Groenendijk et al. (2011) the parameters of a photosynthesis model are optimised using EC data from several Fluxnet sites. Similarly, studies like Kuppel et al. (2012) and Raoult et al. (2016) have constrained the parameters of a global ecosystem model using multi-site EC data. Considering these studies and the results of Kallingal et al. (2023), we hypothesise that assimilating daily CH_4 multi-site field observations using the GRaB-AM framework can derive a set of optimised general parameters capable of representing various types of northern wetlands.

https://doi.org/10.5194/egusphere-2024-373
Preprint. Discussion started: 28 February 2024

The present study's objective is to investigate the capacity of the GRaB-AM framework developed by Kallingal et al. (2023) for calibrating process model parameters in a more general multi-site framework. We aim to optimise selected model parameters for examining to what extent this optimisation improves the model's ability to simulate the seasonal cycle of CH_4 from different wetlands over northern latitudes above 40° N. We also aim to estimate the model process and parameter correlations and uncertainties. The 14 sites chosen for this study were selected to encompass diverse bioclimatic and geographical characteristics of wetlands. This deliberate selection aimed to endow the optimised parameters with the ability to represent a range of wetland types, independent of their distinct climatic and geographical features. We then perform additional validation simulations to evaluate the performance of the calibrated model against 5 different, independent validation sites to verify our above mentioned hypothesis. In the following, we first give a brief overview of the LPJ-GUESS model, the data used in the assimilation and the data assimilation methodology itself. The assimilation results are then presented and discussed in Sect. 3 before we end with the conclusions (Sect. 4).

2 Data and methodology

2.1 LPJ-GUESS model

LPJ-GUESS represents the structure and dynamics of terrestrial ecosystems from local to global scales (Smith (2001), Smith et al. (2014)). The model combines basic eco-physiological features with detailed vegetation dynamics and canopy structure as used in forest gap models, and includes an interactive nitrogen cycle (Smith et al., 2014). In version 4.1, which we used for this study, global vegetation is grouped into thirteen different co-occurring mixtures of Plant Functional types (PFTs) and 5 additional PFTs that can only exist on peatland stands. The model input data consists of climate parameters (mean daily air temperature, precipitation and incoming shortwave radiation), atmospheric CO_2 concentrations and soil properties. LPJ-GUESS simulates vegetation dynamics, ecosystem biogeochemistry, water cycling and energy and carbon fluxes on a daily time step. The peatland module in LPJ-GUESS contains detailed representations of wetland PFT characteristics and bio-geochemical processes including, estimation of peat temperature, hydrology and ecosystem exchanges, including CH_4 emissions.

2.1.1 Main process description in CH_4 module of LPJ-GUESS

A detailed description of the wetland and CH_4 emissions module is given in Wania et al. (2010) and in Kallingal et al. (2023). Here, we only briefly summarise the most important aspects of the module. The wetland peat in LPJ-GUESS is 1.5 m deep and is divided into an acrotelm of thickness 0.3 m with varying water table depth (wtd), and a permanently saturated catotelm. Peat hydrology and peat temperature in this layered structure depend on its composition and prevailing meteorological conditions. The five types of PFTs implemented in the wetlands are Sphagnum mosses, C_3 graminoids, evergreen and deciduous shrubs and a generic herbaceous cushion lichen moss PFT. Shade mortality, inundation stress and daily desiccation stress are limiting factors for the existence and productivity of these PFTs.

https://doi.org/10.5194/egusphere-2024-373
Preprint. Discussion started: 28 February 2024

A potential soil carbon pool distributed in proportion to the root distribution for methanogens to produce CH_4 is the basic concept of the CH_4 module in LPJ-GUESS. The carbon in the soil is transformed to CH_4 or CO_2 depending on the hydrological conditions. A fraction of the produced CH_4 is in dissolved form and the remainder is in gaseous form. A part of this CH_4 is oxidised by the oxygen in the soil and the other part is eventually transported to the atmosphere through either diffusion, plant-mediated transport or ebullition. As shown in Eq.1 the sum of the emissions through these three pathways constitutes the total CH_4 flux from the soil to the atmosphere (Wania et al. (2010), Kallingal et al. (2023)).

$$F_{CH_4} = CH_{4diff} + CH_{4plant} + CH_{4ebul} \quad (1)$$

where F_{CH_4} is the total CH_4 flux, CH_{4diff} is the CH_4 flux component from diffusion, CH_{4plant} is the CH_4 flux component from plant-mediated transport and CH_{4ebul} is the CH_4 flux component from ebullition.

2.1.2 Parameter selection

The parameters selected for optimisation in this study are shown in Table 1. For this study we have considered 10 out of 11 parameters calibrated by Kallingal et al. (2023) in their single-site optimisation. The parameter w_{tiller} is removed because it showed high correlation with r_{tiller} in Kallingal et al. (2023).

Table 1. Parameters selected for the multi-site assimilation. Model prior values, prior standard deviation (std), units, and description of the parameters are given.

Number	Parameter	Prior value	Prior std	Unit	Description
1.	R_{moist}	0.4	0.396	-	Moisture response in acrotelm
2.	CH_4/CO_2	0.085	0.236	-	CH_4 to CO_2 ratio
3.	f_{oxid}	0.5	0.36	-	Litter CO_2 fraction
4.	ϕ_{tiller}	70	36	%	Porosity of tiller
5.	r_{tiller}	0.0035	0.004	m	Radius of Tiller
6.	f_{air}	0	4	%	Fraction of air in peat
7.	por_{acro}	0.98	0.06	-	Acrotelm porosity
8.	por_{cato}	0.92	0.076	-	Catotelm porosity
9.	$R_{moist\text{-}an*}$	0.025	0.04	-	Moisture response in catotelm
10.	λ_{root}	25.17	12	cm	Decay length of root biomass

2.2 Flux sites and climate data

As mentioned above, for this study we selected 14 natural wetland sites for the assimilation and 5 additional wetland sites for validation (see Fig. 1, Table 2 and Table 6). The selection criteria for the sites were: 1) that they are located above 40°North, 2) that they include at least three years of consecutive CH_4 (at least the summer) measurements and meteorological measurements

https://doi.org/10.5194/egusphere-2024-373
Preprint. Discussion started: 28 February 2024

available for the sites used for assimilation and same criteria, but, at least two years of measurements available for the sites used for validation, and 3) that they represent arctic, boreal or temperate ecosystems. We did not consider lakes, uplands, etc. as they are beyond the scope of the present study. The nineteen sites are representative for a range of wetland types including fens, mires, bogs, marshes and a wet tundra (for validation).

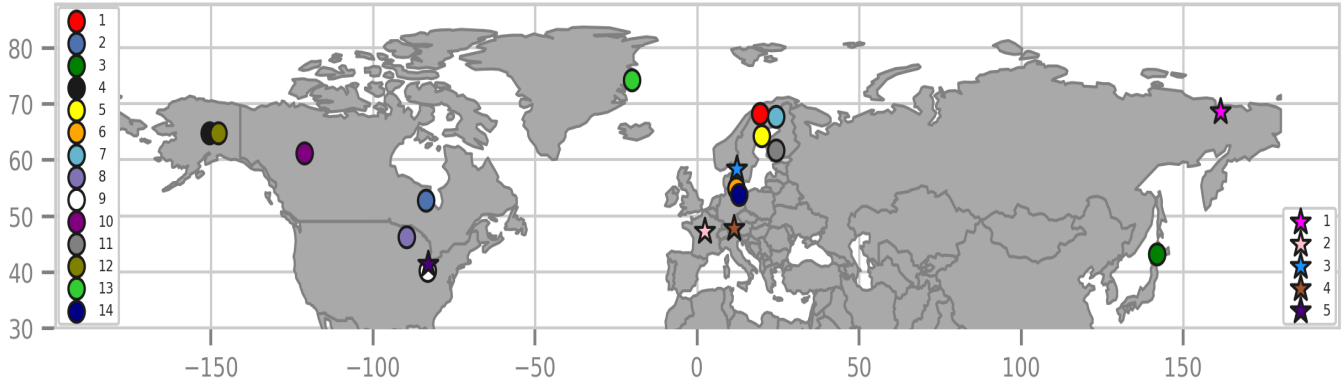

Figure 1. Location of measurement sites selected for the study. The 14 sites used for assimilation are indicated as circles and the 5 sites used for validation are indicated as stars. The numbers in the left and right side legends correspond to the numbers assigned to the sites in Table 2 and Table 6, respectively.

In total we have used 18,437 data points of daily CH_4 measurements for assimilation, spanning approximately 93 measurement-years. We did not consider any sites where the climate data had gaps of more than fourteen days. In case of gaps smaller than fourteen days the data are back-filled (by copying the values from the preceding cells) to ensure dataset continuity, as data with gaps cannot be used in the model as input. For validation, we utilised 5111 data points spanning a total of 14 measurement years. For all sites, only the available CH_4 observations are compared with the model both for assimilation and validation, i.e., we do not use any gap-filled data. It should be noted that for the assimilation sites Att, Bon, Sco, Uoa, and Zak, most of the data from winter months were missing, while for the validation sites Lgt and Wpt, most of the data from summer months were missing. We assume that the missing winter data from the sites used for assimilation will not introduce considerable bias, as the model simulates almost zero emissions during winter.

https://doi.org/10.5194/egusphere-2024-373
Preprint. Discussion started: 28 February 2024

Table 2. Site information and data references of the 14 natural wetland sites used for assimilation. MAT refers to the mean annual temperature and MAPr to the mean annual precipitation. For Bib, Deg, Lom, Los, Ole, Sco, Sii, and Uao MAT and MAPr are extracted from the corresponding grid cells of the site locations of the WorldClim 2.0 gridded product (Fick and Hijmans, 2017), and for the rest of the sites, the information is taken from their references. The table also includes type, coordinates and climate zones of the wetlands, as well as the time period of data availability.

No	Site	Abr.	Type	Location	Climate Zone	MAT (°C)	MAPr (mm)	Period	Reference
1.	Abisko	Abi	Bog	68.21°N, 19.03°E	Arctic	-0.7	304	2014-18	Łakomiec et al. (2021)
2.	Attawapiskat	Att	Fen	52.70°N, -83.95°E	Boreal	-1.3	700	2011-20	Todd and Humphreys (2018)
3.	Bibai	Bib	Bog	43.32°N, 141.81°E	Temperate	6.7	1153	2015-19	Ueyama et al. (2020)
4.	Bonanza Creek	Bon	Bog	64.69°N, -148.32°E	Boreal	-0.9	331	2014-17	Euskirchen and Edgar (2020)
5.	Degerö	Deg	Fen	64.18°N, 19.55°E	Boreal	1.2	523	2014-19	Granberg et al. (2001)
6.	Huetelmoor	Hue	Fen	54.21°N, 12.17°E	Temperate	10.2	572	2011-19	Koebsch and Jurasinski (2020)
7.	Lompolojänkkä	Lom	Fen	68.00°N, 24.21°E	Boreal	-0.4	484	2006-15	Lohila et al. (2020), Aurela et al. (2015)
8.	Lost Creek	Los	Fen	46.08°N, -89.97°E	Temperate	4.8	833	2014-19	Desai and Thom (2020)
9.	Olentangy	Ole	Marsh	40.02°N, -83.01°E	Temperate	12.1	1120	2011-16	Bohrer and Morin (2020)
10.	Scotty Creek	Sco	Bog	61.30°N, -121.29°E	Boreal	-2.8	414	2014-18	Sonnentag and Helbig (2020)
11.	Siikaneva	Sii	Fen	61.83°N, 24.193°E	Boreal	4.2	707	2005-15	Rinne et al. (2018)
12.	Uni. of Alaska	Uoa	Bog	64.86°N, -147.85°E	Boreal	-2.9	611	2011-19	Iwata et al. (2020)
13.	Zackenberg	Zak	Fen	74.30°N, -20.30°E	Arctic	-8.6	253	2006-20	Scheller et al. (2021)
14.	Zarnekow	Zar	Fen	53.87°N, 12.88°E	Temperate	9.7	426	2014-19	Sachs et al. (2020)

2.3 Data assimilation system

To find an optimal posterior parameter set we used an adaptive Rao–Blackwellised Markov Chain Monte Carlo Metropolis-Hastings (MCMC-MH) algorithm (Andrieu and Thoms, 2008) to iteratively reduce a so-called cost function (see Eq. 2) that compares the modelled observable with the observations. The details of this search algorithm and its application to a single-site optimisation have been described in Kallingal et al. (2023). Efficient sampling from the target distribution requires a proposal distribution that correctly represents the dependence structure of the target, and to avoid manual tuning of the proposal we use an adaptive MCMC to tune the proposal distribution, where the Rao–Blackwellisation improves the adaptation step. The tuning improves the MCMC convergence speed and avoid cases of incomplete convergence (Andrieu and Thoms, 2008), especially for a complex non-linear model like LPJ-GUESS.

We assumed errors in observation and parameters in the form of Gaussian distributions yielding the cost function J (x),

$$J(x) = \frac{1}{2}\sum_{i=1}^{n}(Y_i - M_i(x))^t R_i^{-1}(Y_i - M_i(x)) + \frac{1}{2}(x - x_p)^t B^{-1}(x - x_p) \quad (2)$$

where Y_i are the CH_4 observations at the i^{th} site, $M(x)$ is the simulated CH_4 values from LPJ-GUESS given parameters x, R is the covariance matrix of the observation errors, x_p are the expected prior parameters and B is the prior parameter error

https://doi.org/10.5194/egusphere-2024-373
Preprint. Discussion started: 28 February 2024

covariance matrix. Thus the first term represents the model-data misfit weighted by the observation error covariances and the second term represents the prior information on the parameters weighted by the parameter error covariances.

Samples are generated by drawing x_{prop} from a proposal distribution and then either accepting the proposed state ($x_i = x_{\text{prop}}$) or keeping the current state ($x_i = x_{i-1}$) based on the posterior probabilities. The probability of accepting the proposed state (α) is generally computed as

$$\alpha = \min\left(1, \frac{P(x_{\text{prop}})}{P(x_{i-1})}\right) \tag{3}$$

Here, $P(x_{\text{prop}})$ is the posterior probability of the proposed state, and $P(x_{i-1})$ is the posterior probability of the current state, both computed using the cost function, Eq. 2. The acceptance probability ensures a balanced exploration of the parameter space, accepting states that improve the fit while allowing occasional exploration of less favorable regions (see Andrieu and Thoms (2008) for technical details and Kallingal et al. (2023) for the implementation).

Table 3. Data availability and threshold estimated for the base error values. The number of available observations from each site is also provided.

No	Site	Threshold for base error ($gC\ m^{-2}d^{-1}$)	No. of obs.	Available data (%)	Error below the threshold ($gC\ m^{-2}d^{-1}$)
1.	Abi	0.003	1310	89.7	0.09
2.	Att	0.0012	1952	61.65	0.036
3.	Bib	0.01	815	60.1	0.3
4.	Bon	0.01	560	60.0	0.3
5.	Deg	0.0057	1361	74.6	0.15
6.	Hue	0.037	2124	76.4	1.1
7.	Lom	0.011	1682	51.3	0.32
8.	Los	0.0085	1472	83.0	0.25
9.	Ole	0.0085	1135	74.6	0.25
10.	Sco	0.018	646	49.5	0.53
11.	Sii	0.01	1547	44.1	0.3
12.	Uao	0.013	1126	41	0.38
13.	Zak	0.007	1294	26.67	0.21
14.	Zar	0.04	1413	77.42	1.2

For optimisation we used the GRaB-AM with a chain length of 100,000 iterations, where each iteration involves one complete model run for all 14 sites. As mentioned above, daily averages of observations collected from the above-mentioned 14 sites are assimilated simultaneously. For each site only the actual observations, i.e., not gap-filled data are used to calculate the cost function.

Considering the difficulty of calculating error correlations in the observations, we only considered errors in individual observations, i.e., we did not consider off-diagonal elements in specifying the observational error covariance matrix R in the

https://doi.org/10.5194/egusphere-2024-373
Preprint. Discussion started: 28 February 2024

cost function (Eq. 2). Estimating the exact observation error for each site is again challenging. Assigning a constant percentage error for all measured values could introduce a bias, as it would result in high error values for measurements with high magnitudes and very low error values for observations with small magnitudes. To overcome this challenge, we followed the procedure introduced by Knorr and Kattge (2005) for the case of assimilating CO_2 eddy covariance observations and assign a threshold value set at 5% of the variance of the distributions of observations, calculated separately for each site. Values below this threshold are identified, and a uniform error is assigned to them (see Table 3) . An error of 30% is estimated for the observations greater than the threshold values. For the matrix B in the Eq. 2, for each parameter a standard deviation of 40% of their possible range is assumed based on the expertise of LPJ-GUESS modellers.

2.4 Posterior estimation

After completing a full run of the chain, the posterior parameter error covariance matrix (Bp) is estimated from the prior error covariance matrices of the observations, R, and of the parameters, B, and the linearisation of the model fat the minimum of the cost function, $J(M_\infty)$, as described in Tarantola (1987).

$$Bp = [M_\infty^t R^{-1} M_\infty + B^{-1}]^{-1} \tag{4}$$

Bp is then used to estimate the level of optimisation of each parameter and the sensitivity of the cost function to them. The posterior parameter uncertainties have been estimated from the square root of the diagonal elements of Bp. Large absolute values of posterior error correlations indicate that the observations do not provide independent information to distinguish the effects of a given parameter pair (Tarantola, 1987).

From the 100,000 samples yielded by the GRaB-AM framework 75% of this chain was discarded as burn-in. The remaining part of the chain, which we consider as converged to its stationary distribution was used for calculating the Maximum a Posteriori estimation (MAP) and posterior mean estimations. The posterior distributions of parameters are classified as 'well-constrained', 'poorly constrained', and 'edge-hitting' parameters. The well-constrained parameters are characterised by a clearly defined unimodal distribution with a low standard deviation. Conversely, poorly constrained parameters exhibit a relatively flat multimodal distribution with a large standard deviation. For a more precise estimation, we classified posterior parameter distributions as poorly constrained if the standard deviation exceeded 20% of the total range. Edge-hitting parameters cluster near one of the edges of their prior range, as described by Kallingal et al. (2023) and Braswell et al. (2005).

2.5 Experimental setup

The model is spun up for 500 years using available Climate Research Unit (CRU) meteorological forcing data (University of East Anglia Climatic Research Unit , CRU) to bring the model state variables, i.e., the various carbon pools to initial equilibrium. After spinning up, the model was run for the 14 study sites using local, daily meteorological forcing data collected directly at the sites. We have bias-corrected the CRU data for the gridcells in which the sites are located to enforce agreement with monthly mean values of the site-specific meteorological input data. For this we have used at least two years of

https://doi.org/10.5194/egusphere-2024-373
Preprint. Discussion started: 28 February 2024

meteorological data that are recorded prior to the time period of the site observations that we used for the assimilation. Daily measurements of air temperature, precipitation, and incoming short-wave radiation collected at the wetland are used to input the model. Atmospheric CO_2 concentration, as described in McGuire et al. (2001) and updated until recent years using data from the NOAA Global Monitoring Laboratory (NOAA-GML) is used as the CO_2 concentration input to the model.

Most of the CH_4 observations at the sites were available with a half-hourly resolution, but for the assimilation we used daily mean values corresponding to the LPJ-GUESS temporal resolution. Also, using daily values reduces the complexity of error correlations of half-hourly data and is better suited for a broad range time scale assimilation (Lasslop et al., 2008). Days with less than 50% of half-hourly CH_4 data availability were removed from the assimilation.

3 Result and discussion

The GRaB-AM algorithm incorporates the adaptation mechanism with Rao-Blackwellisation, which recursively updates the covariance of the proposal distribution to capture the dependence among different parameters. In theory, this will improve the efficiency of MCMC by allowing the proposal distribution to take larger steps, while still accounting for parameter inter-dependencies; important particularly for high-dimensional and correlated parameter spaces. In the optimisation process laid out here, with observations from multiple sites and with high-dimensional parameter spaces and a highly non-linear model, the GRaB-AM algorithm is particularly beneficial because it enhances the exploration of a wider parameter space while adapting the proposal distribution over iterations. Having multiple sites in this framework, one crucial challenge was scaling the cost function to maintain a balanced representation of each site's contribution to the overall model-data misfit. This process is particularly relevant when sites exhibit variations in the magnitude of their individual cost functions or when the number of observations at each site differs significantly. Here, the scaling factors are carefully chosen to ensure an approximately equal representation of all sites in the cost function, regardless of their individual characteristics, and to ensure that each site has an equal influence on the optimisation outcome. This study undertook an in-depth examination of posterior parameter distributions, correlations between posterior parameters, and correlations of flux components.

3.1 Posterior parameter distributions

The posterior Probability Density Functions (PDFs) of the parameters from the MCMC chains after the burn-in are displayed in Fig. 2. All parameters, except for ϕ_{tiller}, f_{air} and por_{acro}, are well-constrained with only one peak in the PDF. However, the parameters ϕ_{tiller} , f_{air} and por_{acro} are rather poorly constrained, exhibiting some clustering around multiple peaks in the PDF and having large standard deviations (see Fig. 2).

Except for λ_{root}, none of the parameters exhibited edge-hitting behaviour, indicating that the hypothetical boundaries assigned for each parameter align well with the model structure. The parameter λ_{root} finds its solution nearly at the lower edge. Most parameters displayed posterior solutions far from their prior values, i.e., the prior values where outside the posterior mean estimate $\pm 1\sigma$, except for ϕ_{tiller}. For ϕ_{tiller}, both the MAP and posterior mean appeared close to the prior value, i.e., within 1σ of the posterior mean estimate. Overall, the posterior parameter distributions indicate a successful search within the permitted

https://doi.org/10.5194/egusphere-2024-373
Preprint. Discussion started: 28 February 2024

parameter ranges. The R_{moist}, f_{air}, and λ_{root} showed high skewness and kurtosis. However, the smaller kurtosis values of f_{oxid}, por_{cato}, and $R_{moist_{an}}$, along with their low skewness, indicate that they closely resemble Gaussian distributions. The remaining four parameters showed low skewness, suggesting agreement with a Gaussian distribution, but with very low kurtosis indicating somewhat flatter distributions than a Gaussian distribution.

3.2 Posterior parameter estimates and cross-correlation

The posterior parameter values estimated from the MAP and the posterior mean estimate, along with their standard deviations, are presented in Table 4. A cross-correlation plot (see Fig. 3) shows the correlation between all ten parameter pairs after optimisation to examine potential optimisation issues due to parameter correlation. High positive or negative correlations suggest that these parameters may convey similar information, and one of them might be redundant in further studies. The results show that not many parameters have strong positive or negative correlations, except for the correlation between CH_4/CO_2 and $Rmoist_{\text{an}}$, which has a high negative correlation of -0.82. Many slight positive correlations are observed, with a few pairs like por_{acro} and por_{cato}, por_{cato} and f_{air} having comparatively higher values.

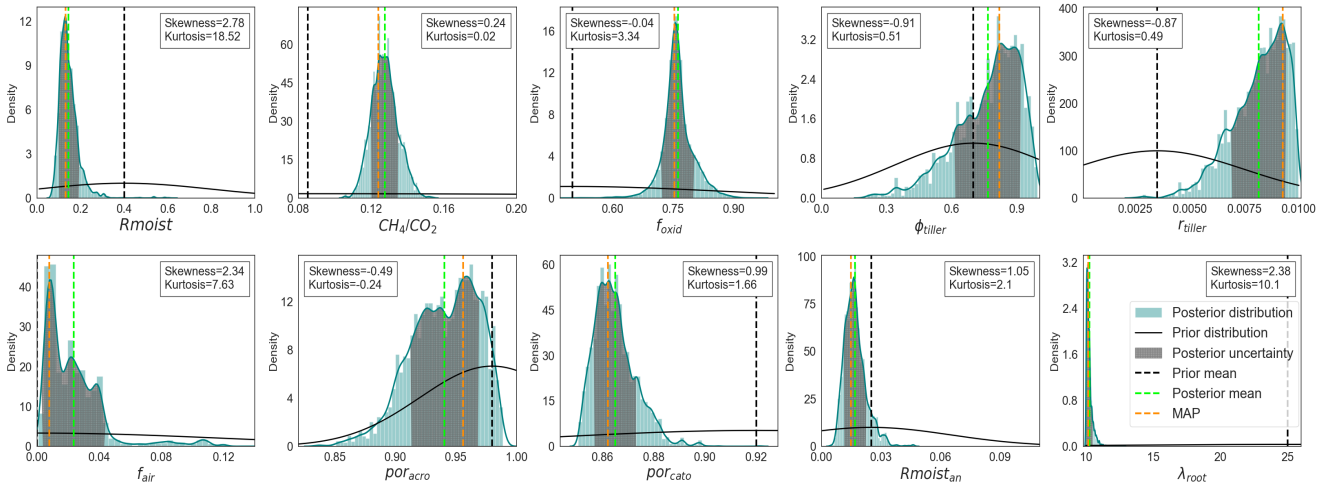

Figure 2. PDFs of the posterior obtained after the GRaB-AM experiment. The blue curves are smoothed Gaussian kernel estimates on the posterior histograms, while the black curves represent the prior distributions. The dotted vertical lines in green, orange, and black correspond to the posterior mean, MAP, and prior means, respectively. The shaded grey area in the distributions represents the 1σ error estimate of the PDFs. Skewness and kurtosis values for each posterior distribution are provided in rectangles.

Rmoist and $Rmoist_{\text{an}}$: These parameters are related to the moisture response in the acrotelm and catotelm, respectively. A smaller value of R_{moist} and $R_{moist_{an}}$ would result in a slower soil carbon turnover time in both aerobic and anaerobic environments, leading to slightly less carbon available for CH_4 production. Although this could decrease the total decomposed carbon in the soil, the strong negative correlation between $R_{moist_{an}}$ and CH_4/CO_2, and the weak negative correlation between R_{moist} and CH_4/CO_2, indicate that the decrease in these parameters has influenced the increase in the CH_4 fraction from this

https://doi.org/10.5194/egusphere-2024-373
Preprint. Discussion started: 28 February 2024

reduced amount of decomposed soil fraction. This indicates that other factors such as water table depth, availability of oxygen, soil temperature, etc., might have influenced the CH_4 production.

CH_4/CO_2: The CH_4/CO_2 was increased to a slightly higher value of 0.14 after the optimisation. This indicates a comparatively higher CH_4 emission fraction from the total decomposed carbon.

f_{oxid}: The fraction of oxidised CH_4, utilising available oxygen in the soil, is represented by the parameter f_{oxid}. The posterior parameter value (0.76) is increased compared to the prior. This indicates that a substantial fraction of the produced CH_4 will get oxidised, while the remaining CH_4 (24%) will get transported to the atmosphere.

ϕ_{tiller} and r_{tiller}: The posterior parameter values estimated for ϕ_{tiller} and r_{tiller} are higher than the prior values, 0.77 and 0.0081, respectively. With aerenchyma tissues having more porous space and a larger radius, the plant-mediated transport of CH_4 to the atmosphere is facilitated. However, through the same spacious aerenchyma tissues, plants also have the potential to transport more O_2 to the soil. This potential increase in the transport of O_2 to the soil could be a reason for increase in f_{oxid}, considering the slight positive correlation observed between f_{oxid} and ϕ_{tiller}.

f_{air}, por_{acro}, and por_{cato}: These three parameters are related to soil composition. The posterior values of f_{air} increased compared to the model prior indicate a higher fraction of air in the soil. The decrease in por_{acro} and por_{cato} indicates decreased porosity in the acrotelm (which can contain both water or air) and catotelm (which can contain only water) respectively. f_{air} and por_{acro} are positively correlated, indicating more air in a more compact acrotelm environment with less water. A higher amount of air in the acrotelm can have a positive effect on diffusion. In the model, the diffusivity of CH_4 in air is estimated to be four orders of magnitude larger than in water. On the other hand, the lower porosity in the catotelm can reduce ebullition due to less water availability that can retain an excess amount of CH_4 and release it when reaching the solubility threshold (see Kallingal et al. (2023) and Wania et al. (2010) for details).

https://doi.org/10.5194/egusphere-2024-373
Preprint. Discussion started: 28 February 2024

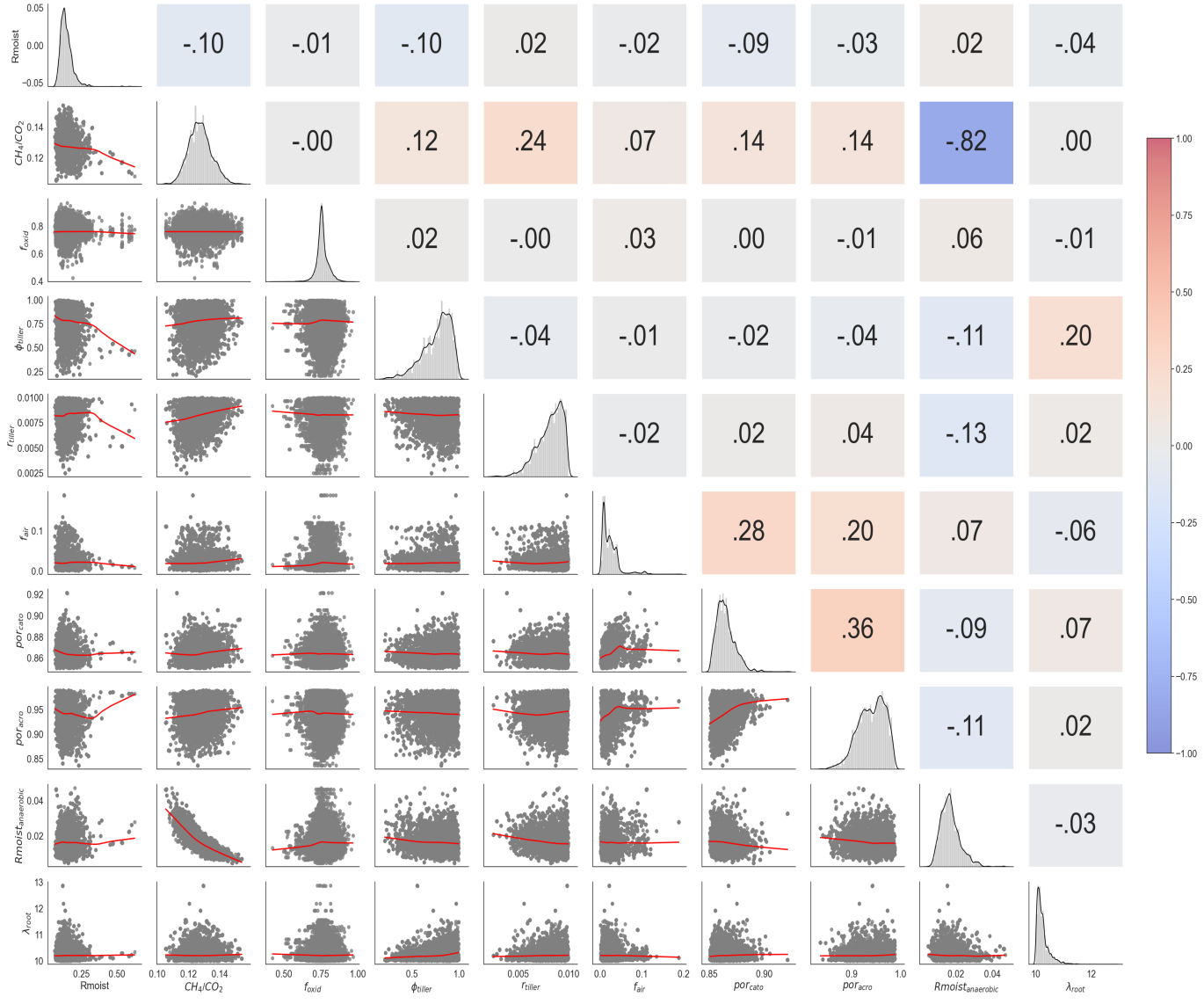

Figure 3. Posterior correlations between parameters derived from the GRaB-AM optimisation. In the upper triangle of the figure, negative correlations are depicted in blue and positive correlations are shown in red. The numerical labels on the upper triangle correspond to values of Pearson's correlation coefficient. The diagonal panels exhibit 1-D histograms for each model parameter. The lower triangle displays two-dimensional marginal distributions for each parameter. The grey dots on the marginal distributions represent the parameter values obtained from the posterior GRaB-AM chain. The ranges of the distributions are labeled on the left and bottom of the figure.

λ_{root}: λ_{root} played a crucial role in this optimisation. After optimisation, this parameter got a significantly lower value of 10.25 cm compared to the prior. It seems that the optimisation, when generally trying to reduce the emission from the model, has a tendency to reduce the decay length of root biomass in the soil. The posterior parameter value closely aligns with the values

https://doi.org/10.5194/egusphere-2024-373
Preprint. Discussion started: 28 February 2024

reported in Kallingal et al. (2023) (10.47 cm). The optimisation results indicate a much shallower soil profile for the majority of root decay activities and CH_4. Given that most of the peat decomposition activities are assumed to occur in acrotelm, the reduction in the magnitude of λ_{root} could substantially facilitate diffusion.

Table 4. Posterior parameter value estimate of the GRaB-AM. The prior values, maximum a posteriori (MAP), posterior mean, posterior standard deviations (std) are given. The cost function values of prior and posterior estimates are also given.

	Parameter										
	R_{moist}	CH_4/CO_2	f_{oxid}	ϕ_{tiller}	r_{tiller}	f_{air}	por_{acro}	por_{cato}	R_{moist_an}	λ_{root}	**Cost value (w)**
Start prior vals.	0.3	0.2	0.6	0.8	0.003	0.001	0.9	0.87	0.04	35	4897.95
MAP	0.13	0.12	0.75	0.82	0.0092	0.008	0.95	0.86	0.017	10.25	221.01
Posterior mean	0.15	0.14	0.76	0.77	0.0081	0.023	0.94	0.86	0.017	10.25	227.30
std ∓	0.045	0.007	0.027	0.15	0.0012	0.02	0.027	0.008	0.005	0.23	

3.3 Performance of the optimisation and cost function reduction

The unweighted cost function values for each of the 14 sites individually and their collective sum, along with the corresponding Root Mean Square Error (RMSE) and χ^2 values, are presented in Table B1 in the appendix. The estimated prior cost function value was 1,763,294.9, and through the optimisation process, it was significantly reduced to 79,296.4 for the posterior mean estimate. This substantial reduction of approximately 95 %, demonstrates the effectiveness of the GRaB-AM algorithm in minimising the cost function. Notably, this successful optimisation occurred even when assimilating data from multiple sites with diverse climatic conditions.

The total reduced chi-square, calculated as twice the value of the cost function divided by the number of observations, has a value of 8.6, indicating a slight underfitting between the model output and observed data accounting for measurement and parameter uncertainty. Notably, none of the sites exhibit overconfidence, as indicated by the individual site χ^2 values larger than 1, with the exception of the site Hue, which shows a χ^2 value below but close to 1 (see Table B1 in the appendix).

The site-wise data-model misfit, presented in terms of RMSE, both before and after optimisation, along with the average RMSE for all sites combined is presented in Fig. 4. Most sites demonstrate a substantial reduction in RMSE, with many achieving over 50 % improvement. This suggests a concerted effort to minimise the misfit, particularly evident in sites such as Abi, Att, Bon, and Uoa, with notable RMSE reductions of 63.5 %, 68.1 %, 70.9 %, and 68.4 %, respectively. These significant reductions imply enhanced accuracy in the model predictions. However, the persistence of model-data misfit is highlighted by the elevated χ^2 values for these sites, namely 22.6, 20.3, 6.8, and 9.2, respectively in the posterior estimate (Table B1 in appendix). The sites Hue, Sco, and Zak have shown the smallest RMSE reduction, but the low χ^2 value indicates a consistent

https://doi.org/10.5194/egusphere-2024-373
Preprint. Discussion started: 28 February 2024

fit to the observation given the assumed uncertainties. The result indicates that attention should be given to the sites with smaller RMSE and bigger χ^2 values, such as Bib, Lom, Ole, Sii, and Zar, as there might be a possibility to further improve them. Overall, the optimisation successfully reduced the model-data misfits, with some variations in the degree of improvement among different sites. Additionally, the substantial reduction in the total cost function, RMSE and χ^2 values from the prior to the posterior indicate an overall improvement of the model.

Even though no correlations are observed between the types of wetlands and their locations, we note that the sites that showed a considerable reduction in RMSE, such as Abi, Att, Bon, Deg, Lom, Los, Sii, Uoa, and Zar, are those that are boreal or arctic in nature, missing only Sco and Zak. Except for Los, all sites located in the temperate region, namely Hue, Ole, Bib, and Zar, showed comparatively lower reductions in RMSE (see Table 2 and Fig. 4).

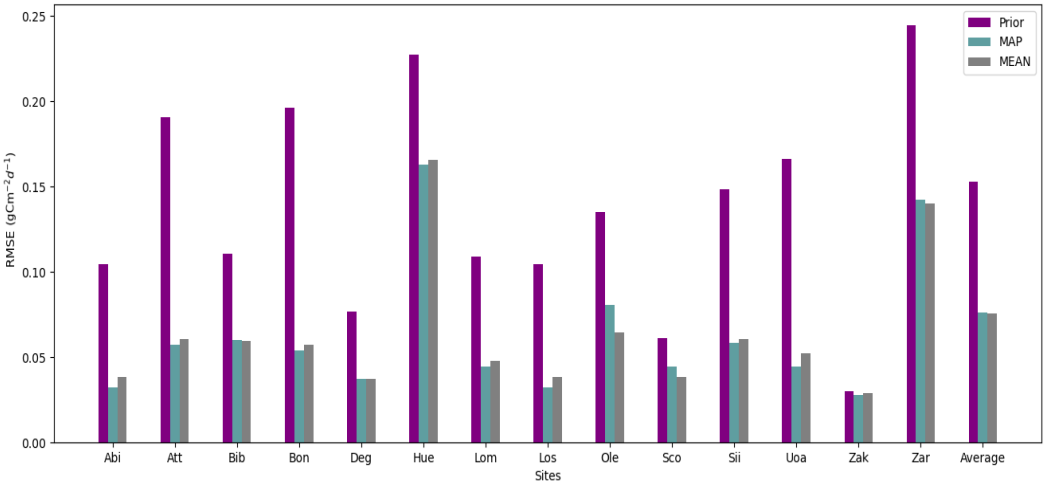

Figure 4. Prior and posterior Root Mean Square Error (RMSE) estimates are provided for each of the 14 sites individually, along with the combined average values. In the figure, purple, cyan, and grey bars represent the RMSE corresponding to the prior estimate, Maximum A Posteriori (MAP) estimate, and posterior mean estimate, respectively.

3.4 Impact of the optimisation

Time-series of the annual sums of CH_4 emissions at four of the 14 sites used in this study (the time-series of the remaining sites are shown in appendix B2, Fig. B2) are shown in Fig. 6a. It demonstrates the ability of the optimised model to capture the annual budget of these sites, irrespective of geographical, temporal, and climatic variability. All four sites exhibited a better fit to the annual budget after the optimisation. Particularly noteworthy is the site Bib, which had a prior estimation in 2016 significantly deviating from the observed values. This discrepancy was corrected in the posterior estimate, and the annual posterior CH_4 emissions at all four sites align well with the observations after the optimisation. Figure 6b displays the mean annual sums of CH_4 estimated at all 14 sites. The figure illustrates that the highest contribution came from the sites Hue and Zar, which have the highest mean annual temperature (MAT) as compared to other sites. The lowest contributions are from Zak and Abi, which have below-zero MAT. Abi, Att, Los, Ole, Sco, Sii, Uoa, Zak, and Zar showed improvement in the mean

https://doi.org/10.5194/egusphere-2024-373
Preprint. Discussion started: 28 February 2024

annual budgets after the optimisation. The remaining sites did not show an improvement. Sites with a large difference between observed and modeled CH_4 tend to have a biased influence on the total cost estimation based on the magnitude of the difference. This can be observed, for example, for the sites Att, Hue, and Zar that all had a high contribution to the cost value. Although we attempted to overcome this limitation by weighting the individual cost function terms for each site, the optimisation algorithm compromised by finding the best fit for sites like Zar and Hue and hence showing a tendency to offset the sites like Bib, Bon, Deg, Low, Sco.

Table 5 presents the total uncertainty for each site and the total uncertainty estimated for all sites together. This estimation assumes independence between parameter uncertainty and model uncertainty, using the following equation:

$$\sigma_{total} = \sqrt{\sigma^2_{\text{model}} + \sigma^2_{\text{param}}} \tag{5}$$

where σ_{model} is the model structural uncertainty estimated from the standard deviation of the prior and posterior residuals (Desroziers et al., 2005). σ_{param} represents the contribution of parameter uncertainty to the overall uncertainty in observation space, estimated from the 95 % credible interval of the parameters and the standard deviation of total sums of the model prediction by taking into account both the parameter uncertainty from the MCMC sampling and the variability in the model predictions. The calculation is performed as follows:

$$\sigma_{\text{param}} = \frac{\sigma_{\text{predic}}(CI_{\text{upp}} - CI_{\text{low}})}{1.96} \tag{6}$$

where, σ_{predic} is the the standard deviation of total sums of the model prediction over MCMC runs, CI_{upp} and CI_{low} are the upper and lower bounds of the credible intervals of the parameters, and the factor 1.96 is the conversion factor to convert the 95 % credible interval to a standard deviation assuming a Gaussian distribution. The total uncertainty of the posterior CH_4 flux estimates for all the sites together was 0.19 $gCm^{-2}d^{-1}$, whereas for the prior fluxes it was 0.36 $gCm^{-2}d^{-1}$. This results in a reduction of the total uncertainty of around 50 % after the optimisation. Comparing the prior and posterior RMSE (Fig. 4) and the uncertainty reduction, it can be concluded that the more constrained sites, such as Abi, Att, Bon, and Uoa, exhibited high uncertainty reduction. Notably, Abi and Att, which had the highest prior RMSE, showed a reduction of uncertainty of around 95 % and 82 %, respectively. A low reduction in uncertainty was mainly observed in sites that demonstrated a low reduction in RMSE. In Contradiction to this, even though the RMSE reduction observed in the case of Zak is very small, this site showed an uncertainty reduction of around 33 %.

Figure 5 illustrates time-series of observed, prior, and posterior fluxes for all the 14 sites considered in the assimilation. The model adeptly captures the seasonal cycles of CH_4 emissions from all wetlands, both for flux estimates using the prior and the posterior parameter values. Generally, no significant phase shift is observed in either the prior or the posterior estimates. However, for Bib, both prior and posterior estimates exhibit a slight phase shift to early summer, while the sites Hue, Los and Zar show a similar shift to late summer.

The optimisation resulted in a significant reduction in RMSE across all sites. However, emissions at Abi, Att, Los, Ole, Sii, and Uoa sites continued to be overestimated. Notably, the posterior estimations for Abi and Att, major contributors to the total

https://doi.org/10.5194/egusphere-2024-373
Preprint. Discussion started: 28 February 2024

Table 5. Prior and posterior total uncertainty estimates (σ ($gCm^{-2}d^{-1}$)). Total parameter and model uncertainty estimates separately for each site and collectively for all sites combined are shown.

Site	Prior Unc.	Posterior Unc.	Site	Prior Unc.	Posterior Unc.
Abi	0.18	0.01	Los	0.04	0.03
Att	0.11	0.02	Ole	0.02	0.019
Bib	0.08	0.04	Sco	0.10	0.02
Bon	0.15	0.02	Sii	0.05	0.04
Deg	0.03	0.02	Uaf	0.08	0.03
Hue	0.13	0.12	Zak	0.03	0.02
Lom	0.03	0.027	Zar	0.11	0.10
Total Unc.	0.36	0.19			

cost function value, remained considerably distant from the observations. These sites were assigned a high weight for the cost function weighting to represent them in the total cost function but without overemphasising their influence. For Bib (except for 2015), Deg, Hue, and Zak emissions were consistently underestimated. The remaining four sites demonstrated reasonably good agreement of the posterior estimates with the observations. Using the GRaB-AM algorithm at a single site, Kallingal et al. (2023) observed systematic underestimation over many years. Employing multiple sites with varying climatic variability has proven beneficial in resolving this issue, as sites like Bib, Deg, Sco, etc., exhibit both overestimation and underestimation in consecutive years.

https://doi.org/10.5194/egusphere-2024-373
Preprint. Discussion started: 28 February 2024

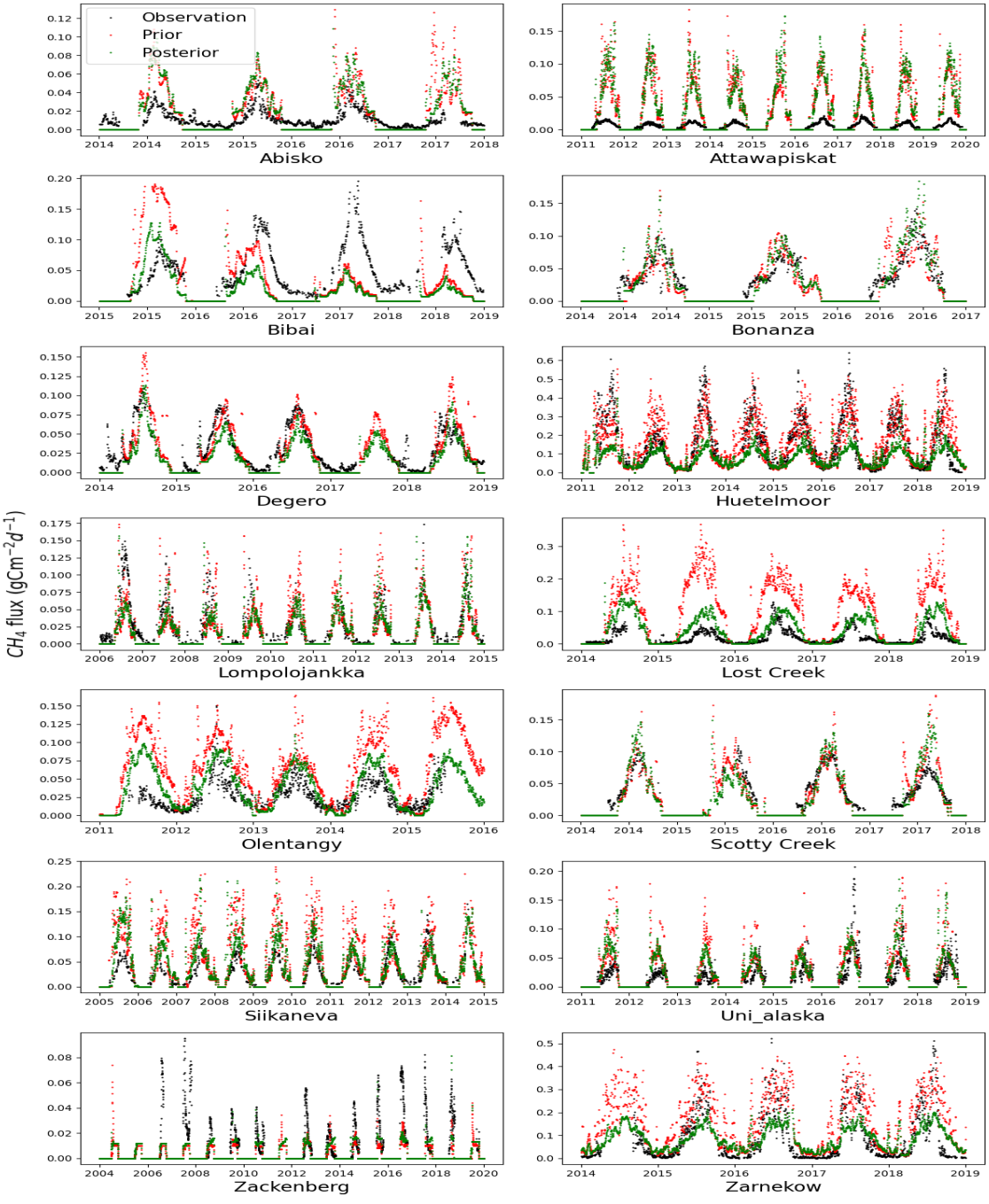

Figure 5. The CH_4 simulation from the LPJ-GUESS model from 14 different wetland sites (green dots) after optimising with the GRaB-AM algorithm. The black dots are the real CH_4 observations from corresponding wetlands. The red dots are the prior simulation with the prior model parameters used to start the MCMC chain. Three days of running averages are calculated from the original time series, and from most of the figure a few outliers on the vertical axis have been removed for better visualisation.

https://doi.org/10.5194/egusphere-2024-373
Preprint. Discussion started: 28 February 2024

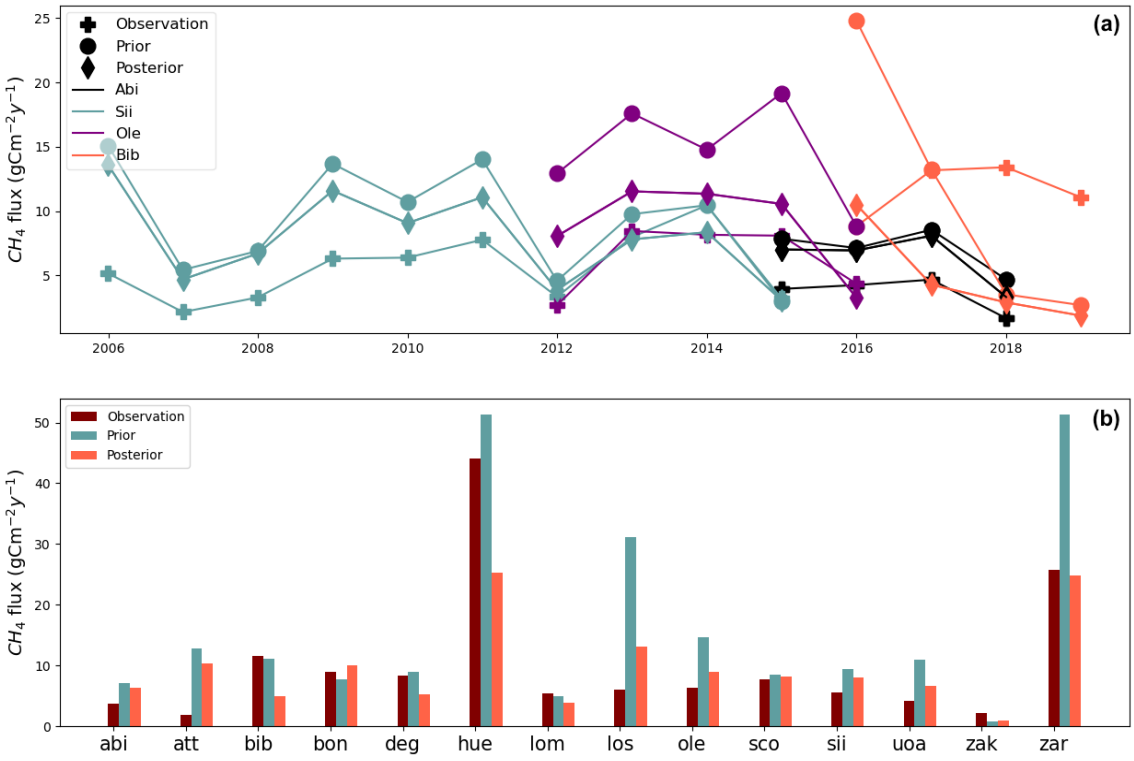

Figure 6. Figure (a) displays the annual sum estimation of CH_4 from four out of 14 sites used in the study. The sites are represented in different clours with distinct markings to distinguish between Observation, Prior, and Posterior. Figure (b) presents the mean annual sums of CH_4 estimated for all 14 sites used in this study as bar charts. It should be noted that the averages of the observations are calculated with only the available daily averages used for the assimilation.

3.4.1 Changes in component contribution

The observed data points available from all 14 sites collectively provide a total of 888.8 gCm^{-2}. The prior sum estimate for the corresponding data points was 1957 gCm^{-2}. This value reduced to 850.9 gCm^{-2} after optimisation, resulting in a slight underestimation of -38.1 gCm^{-2}. Post-optimisation, there was a reduction of approximately 56.52 % from the prior CH_4 flux estimate. Although some underestimation persists, the optimisation demonstrated good performance in estimating the total CH_4 flux.

Changes in the component-wise estimation of ebullition, diffusion, and plant-mediated transport before and after optimisation is illustrated in Fig. 7. The inner circles represent the priors, while the outer circles represent the posterior model estimates. In general, the optimised parameters are constrained differently for different components across sites. No single transport mechanism was dominant after optimisation. Regarding the prior estimate, all sites but Hue and Att had significant contributions from all three emission components. Hue and Att had a very minor contribution from plant-mediated transport. After optimisation, zero contributions from plant-mediated transport were estimated for both these sites. Interestingly, for the

https://doi.org/10.5194/egusphere-2024-373
Preprint. Discussion started: 28 February 2024

site Los, the majority of the prior was contributed by plant-mediated transport and ebullition. However, in the posterior, ebullition contributed very little and was taken over by diffusion. Furthermore, many sites showed the dominance of only two components after optimisation. It was consistently observed that the third component was suppressed, regardless of the nature or climatic conditions of the site.

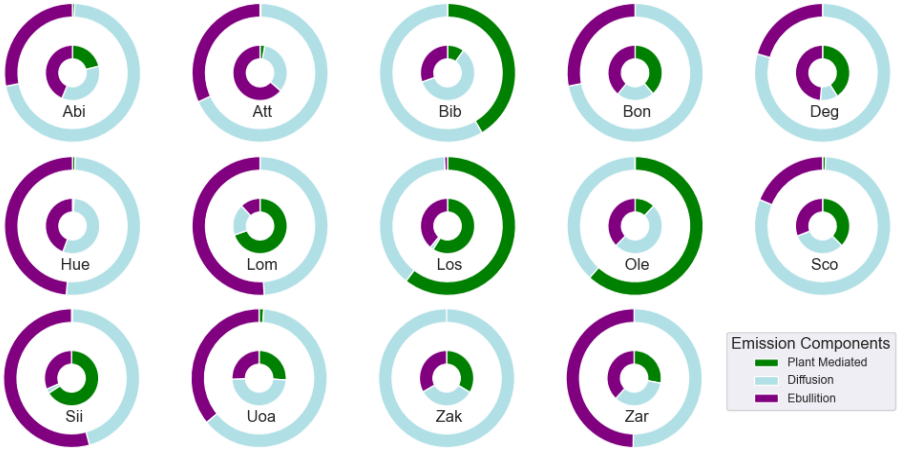

Figure 7. Component-wise percentage contribution of CH_4 to the total modelled emission for all 14 sites is presented separately. The inner circle represents the prior estimate, and the outer circle represents the posterior estimate.

Another interesting observation pertains to the site Zak, an arctic Fen with a very low mean annual temperature (MAT), where nearly equal contributions from all three components were observed in the prior. The posterior, however, showed that nearly all emissions were from diffusion, with very little contributions from the two other components. The RMSE estimate for this site indicates a very low reduction compared to other sites, suggesting that the optimisation did not perform well in constraining this site. The dominance of only one or two components after optimisation suggests biases and highlights the need for improvements in the GRaB-AM algorithm. On the other hand, resolving this issue might be achievable through component-wise assimilation into the model using data from all three components and local hydrology observations. However, this will be challenging due to the unavailability of data, especially of the ebullition. Measuring ebullition fluxes poses significant challenges, primarily attributed to the pronounced spatiotemporal variability. Ecosystems exhibit rapid, momentary surges in fluxes, reaching exceptionally high levels within seconds, interspersed with prolonged periods of negligible ebullition (Canadell et al., 2022).

3.4.2 Summer and winter anomalies

In freshwater wetlands the emission of CH_4 can vary across latitudes based on the growing season and climatic conditions. Assimilating a single site into the LPJ-GUESS model, Kallingal et al. (2023) observed some difficulty in the model's ability to capture winter-time emissions and the tendency to underestimate the summer-emission. The model emitted zero CH_4 when the

https://doi.org/10.5194/egusphere-2024-373
Preprint. Discussion started: 28 February 2024

input temperature dropped below zero. However, observations of CH_4 fluxes indicated that the wetland was still emitting CH_4. Figure 8 illustrates the mean annual summer (April to September) and winter (October to March) emissions (MAS, MAW) for all sites and their corresponding standard deviations and Fig. B1 in the appendix shows 'summer' and 'winter' anomalies. It should be noted that the winter mean and anomaly estimation for the sites Att, Bon, Sco, Uoa, and Zak was conducted with only a very limited number of available data points, as most of them were missing. Conversely, it should be taken into account that proper winter measurements were not carried out at these sites, given the almost negligible emission estimates during the winter months due to their extremely cold temperatures. For all these sites, the mean annual temperature (MAT) was estimated to be below zero (refer to Table 2 and the corresponding site references).

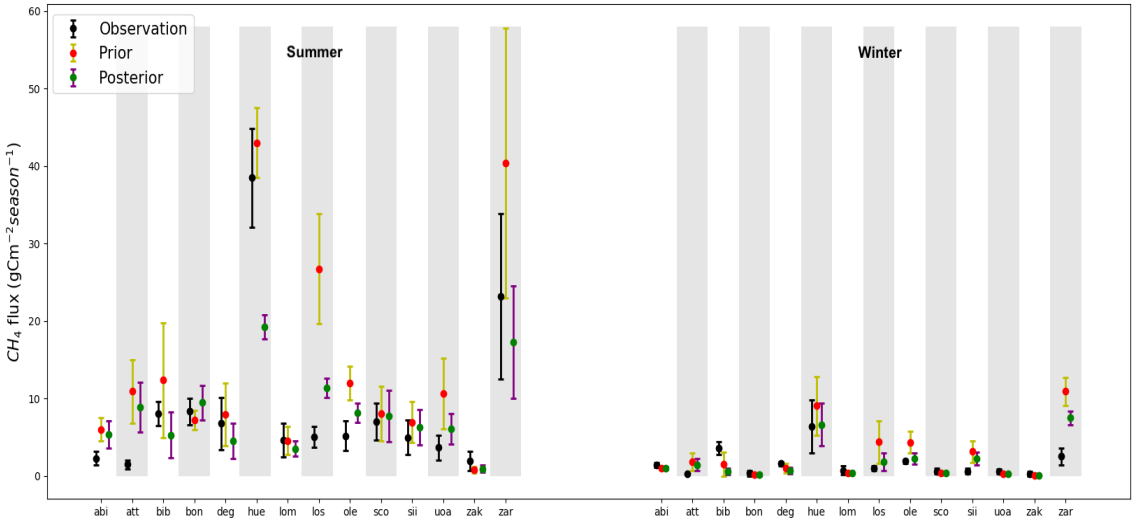

Figure 8. Mean annual summer (MAS, left side) and winter (MAW, right side) emissions for all sites, along with their corresponding standard deviations. The dots represents mean seasonal values, and error lines indicates their 1 standard deviation.

After the optimisation, both MAS and MAW emission estimates for sites Abi, Att, Los, Sco, Sii, and Zar exhibited improved agreement with the observations. The sites Uoa and Bib showed improvement in summer but not in winter whereas the sites Bon, Hue, Lom, and Ole improved in winter but not in summer. The sites Zak and Deg did not show any significant improvement in either season. For the site Deg, the prior estimates were closer to the observations than the posterior, and for the site Zak no significant changes were observed. Summer emissions in Zak were underestimated by both the prior and posterior models. This may be attributed to the relatively low (below zero) mean annual temperature (MAT) of -8.6 at this location and the decomposition seasonality. In contrast, for the sites Abi and Att with negative MAT, the model tends to overestimate summer emissions, the observed average summer emissions were comparatively lower. However, despite a MAT of -2.9 °C at the site Sco and -2.6 °C at the site Uoa, both these sites demonstrated relatively high summer emissions, which were better captured by the model using the posterior parameter values. Sites with a higher MAT, such as Hue, Bib, and Zar, exhibited

https://doi.org/10.5194/egusphere-2024-373
Preprint. Discussion started: 28 February 2024

the highest summer emission values. Although, the site Ole, which has the highest MAT of 12.1 °C, displayed comparatively lower summer emissions. This difference could be influenced by the substantial MAPr of 1120 mm at the Ole site.

For most of the sites, the observed winter annual mean was very close to zero, except for Bib, Deg, Hue, Ole, and Zar. For Hue, Ole, and Zar, the posterior estimate showed better performance in capturing the seasonal trends in observations than the prior. The site Hue exhibited high winter emissions. When the air temperature input for this site was estimated, it showed a mean value of 3.8 °C in winter months. Overall, although the majority of sites showed improved estimation of winter and summer emissions, some of the sites remained unchanged or did not perform better than before. The estimation of the standard deviation for summer and winter months showed a reduction for all sites after optimisation.

3.5 Validation of optimisation

When optimising model process parameters using observations from multiple sites in the assimilation, it is essential to assess whether the posterior set of parameters can enhance the model performance for other wetlands within the study area limit. This assessment involves using additional observations which are not used in the assimilation process. Data from 5 different wetlands located in various parts within the study area limit are used to estimate the impact of the optimised parameters on the overall model performance (See Sect. 2.2 and Table 6).

Table 6. Site information and data references of 5 natural wetland sites used for validation. MAT refers to the mean annual temperature and MAPr to the mean annual precipitation collected from their references. The table also includes the time period of data collected, the availability of data and the type and climate zones of the wetlands.

No	Site	Abr.	Type	Location	Climate Zone	MAT (°C)	MAPr (mm)	Period	No. of Obs.	Available Data (%)	Reference
1.	Chersky	Che	Wet Tundra	68.61°N, 161.35°E	Arctic	-9.8	200	2014-2017	923	84	Merbold et al. (2020)
2.	La Guette	Lgt	Fen	47.32°N, 2.28°E	Temperate	11.07	650	2017-2019	227	31	Jacotot et al. (2020)
3.	Mycklemossen	Myk	Bog	58.36°N, 12.16°E	Hemi-boreal	6.9	802	2016-2019	1095	100	White et al. (2023)
4.	Schechenfilz N.	Sfn	Bog	47.80°N, 11.32°E	Temperate	8.28	700	2012-2015	700	64	Schmid and Klatt (2020)
5.	Winous Point N.	Wpt	Marsh	41.48°N, -82.99°E	Temperate	11.4	900	2011-2014	477	44	Chen and Chu (2020)

As mentioned in Sect.2.2, the primary criterion for selecting the 14 sites used in this study was to ensure representation of various wetland bioclimatic and geographical attributes, including temperature, moisture, and vegetation-related parameters, across arctic, boreal and temperate regions. Through this selection, we aimed to equip the optimised parameters with the capability to accurately represent different types of wetlands, irrespective of their specific climatic and geographical features. Our validation analysis suggests that the optimised parameters successfully achive the aforementioned goal.

https://doi.org/10.5194/egusphere-2024-373
Preprint. Discussion started: 28 February 2024

Table 7. RMSE reduction and the percentage change in the total emission estimate (in %) for the validation sites, along with their prior and posterior uncertainty (σ) estimates.

Site	RMSE Reduction (%)	Change in Total Estimation (%)	Total Prior σ	Total Posterior σ $gCm^{-2}d^{-1}$
Che	31.2	-21.5	0.29	0.19
Lgt	0.6	4.9	0.10	0.10
Myk	59.8	43.6	0.17	0.09
Sfn	81.1	38.5	0.77	0.16
Wpt	-0.23	31.8	0.2	0.18
Total	58.8	19.2	0.61	0.17

Among the sites used for validation, four out of 5 sites showed a considerable reduction in RMSE (Table 7). The site Wpt, a temperate marsh, exhibited a very slight increase in RMSE. The total prior model-data mismatch of CH_4 estimated at this site during the time period was 72.5 gCm^{-2}, which increased to 78.98 gCm^{-2} after optimisation. Despite the lack of improvement, the total σ estimated after optimisation was slightly less than the prior. Wet tundras were not used for assimilation; however, the site Che, a wet tundra used for validation, demonstrated a remarkable 31.2 % reduction in RMSE with a 21.5 % increase in posterior estimation compared to the prior. Moreover, there was a significant reduction in total posterior σ, decreasing from 0.29 to 0.19. A collective 58.8 % reduction in RMSE was observed for all sites together, with a posterior total σ of 0.19. The most significant change was contributed by Sfn and Myk, which are temperate and hemi-boreal fens, respectively. This makes it interesting, as in general, boreal and temperate fens were the least constrained during the optimisation.

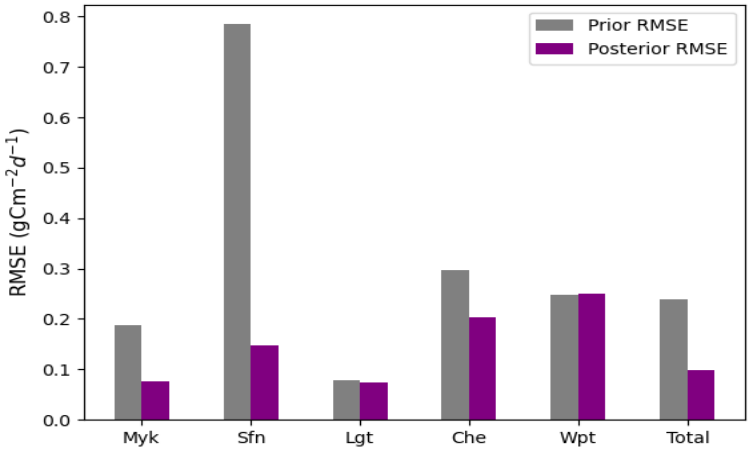

Figure 9. Prior and posterior Root Mean Square Error (RMSE) estimates are provided for each of the 5 validation sites individually, along with the combined average values. Purple, and grey bars represent RMSE corresponding to the prior estimate and posterior mean estimate, respectively.

https://doi.org/10.5194/egusphere-2024-373
Preprint. Discussion started: 28 February 2024

Overall, the results from validation sites indicate that the optimised parameters perform better in representing different types of wetlands, especially for bogs. The total estimation of observed CH_4 from all the sites during the specified time period is 319 gCm^{-2}. The posterior estimate for the same period was 421 gCm^{-2}, resulting in a mismatch of 102 gCm^{-2}. Given this observation and the less constrained nature of sites like Wpt and Lgt, which are temperate, future studies might consider the necessity of different parameter sets for different wetland types. It is worth noting that the majority of temperate sites used for optimisation also exhibited lower level performance in terms of cost reduction (see Sect. 3.3).

4 Conclusions

This study aimed to optimise the simulation of CH_4 emissions from natural wetlands in the LPJ-GUESS DGVM using eddy-covariance flux measurement data obtained from 14 diverse natural wetlands, characterised by variations in temporal, spatial, and/or climatic features. Ten selected model process parameters with the greatest influence on wetland CH_4 flux simulation are optimised using the Global Raoblackwellised Adaptive MCMC (GRaB-AM) algorithm within a Bayesian framework as a follow-up study of Kallingal et al. (2023). GRaB-AM is computationally intensive and in this study it took around 480 computational hours to complete the 100,000 iterations on an AMD Ryzen Threadripper processor. Following the optimisation, the study used observations from 5 different wetlands, which again differ in their temporal, spatial and bioclimatic features, to validate the results of the optimisation. The optimisation results showed a substantial enhancement in the model's capacity to align with observed CH_4 fluxes, with a total reduction of approximately 50 % in RMSE and an approximately 53 % reduction in total uncertainty. The discrepancy between the modelled and observed values decreased from 1068.5 gCm^{-2} to 38.1 gCm^{-2}. Validation results demonstrate that four out of 5 sites reduced RMSE, contributing to an overall reduction of approximately 58.8 %. Given the remaining mismatches between observations and simulations and the presence of less constrained sites, future investigations will focus on individual sites, and grouping them based on their bio-geo-climatic characteristics, to examine if they need to be parameterised with different sets of parameters. Additionally, further studies are planned to quantify CH_4 emissions from boreal and temporal wetlands on large spatial scales, using the optimised parameters, and to validate them against independent atmospheric observations, i.e., atmospheric CH_4 observations provided by the European ICOS observation network. Another intended outcome of this study is to make use of the error correlation derived from the study as prior input to the atmospheric CH_4 inversion model, such as Lund University Modular Inversion Algorithm (LUMIA) (Monteil and Scholze, 2021).

Code and data availability. The GRaB-AM code and data used for this article are available at Zenedo data deposition.The LPJ-GUESS model code can be obtained at LPJ-GUESS. If the site observations are intended to be used for other purposes, we highly recommend contacting the corresponding PIs.

https://doi.org/10.5194/egusphere-2024-373
Preprint. Discussion started: 28 February 2024

Appendix A: Data source description

Among the sites used for assimilation, Bib, Bon, Deg, Hue, Los, Ole, Sco, Uoa, USA, and Zar are collected from Fluxnet datasets (Fluxnet, Delwiche et al. (2021)). For the site Abi, CH_4 data is collected from ICOS, and the climate data is obtained from SMHI. Data for Att was collected from Ameriflux. For the site Lom, climate observations of 2006 are taken from the Fluxnet site mentioned above. Observations for the remaining years are obtained from the station Principal Investigator (PI). Precipitation and temperature data for Sii are taken from FMI, and CH_4 data and short-wave radiation data for Sii are collected from AVAA-SMEAR (See Kallingal et al. (2023) for details). For the site Zak, the data was taken from GEM CH_4 and GEM climate.

The data for Che, Lgt, Sfn, and Wpt, used for validation, were collected from the Fluxnet datasets mentioned above. Climate data for Myk was obtained from SITES, and the CH_4 data were obtained from station PIs.

Appendix B: Result of optimisation

Table B1. A comprehensive overview of un-weighted (uw) prior and posterior cost values, RMSE reduction in percentages, and the calculated χ^2 values estimated for all sites individually and together.

Site	Prior cost value (uw)	Posterior cost value (uw)	RMSE reduc. (%)	χ^2 (uw)	Site	Prior cost value (uw)	Posterior cost value (uw)	RMSE reduc. (%)	χ^2 (uw)
Abi	717913.5	14818.9	63.5	22.6	Los	163304.4	8711.5	63.42	11.8
Att	451259.9	19867.7	68.1	20.3	Ole	25368.6	2693.4	52.2	4.7
Bib	54339.3	1274.8	46.0	3.1	Sco	58147.0	644.4	36.7	2.0
Bon	23300.2	1906.2	70.9	6.8	Sii	58183.1	12406.5	59.2	16.0
Deg	10510.6	873.4	51.3	1.3	Uoa	130041.1	5172.5	68.4	9.2
Hue	5033.6	1018.4	27.16	0.96	Zak	3770.6	1357.8	4.3	2.1
Lom	54172.8	7672.8	55.9	9.12	Zar	7949.7	877.3	42.6	1.2
Total	1763294.9	79296.42	50.30	8.6					

B1 Summer and winter anomaly estimation

Summer and winter anomalies of observations, prior, and posterior estimated separately for all 14 sites used can be seen in Fig.B1 . The figure also provides details about the years in which the model either underestimated or overestimated the emissions. It is clear that neither the simulation nor the observation follows any common seasonal patterns or trends. This indicates that CH_4 emissions from wetlands are generally highly dependent on the variabilities in the underlying climatic

https://doi.org/10.5194/egusphere-2024-373
Preprint. Discussion started: 28 February 2024

variables, and the same holds for the model. A detailed analysis of the correlation and sensitivity between the model's CH_4 emission and input climatic variables can be seen in Kallingal et al. (2023).

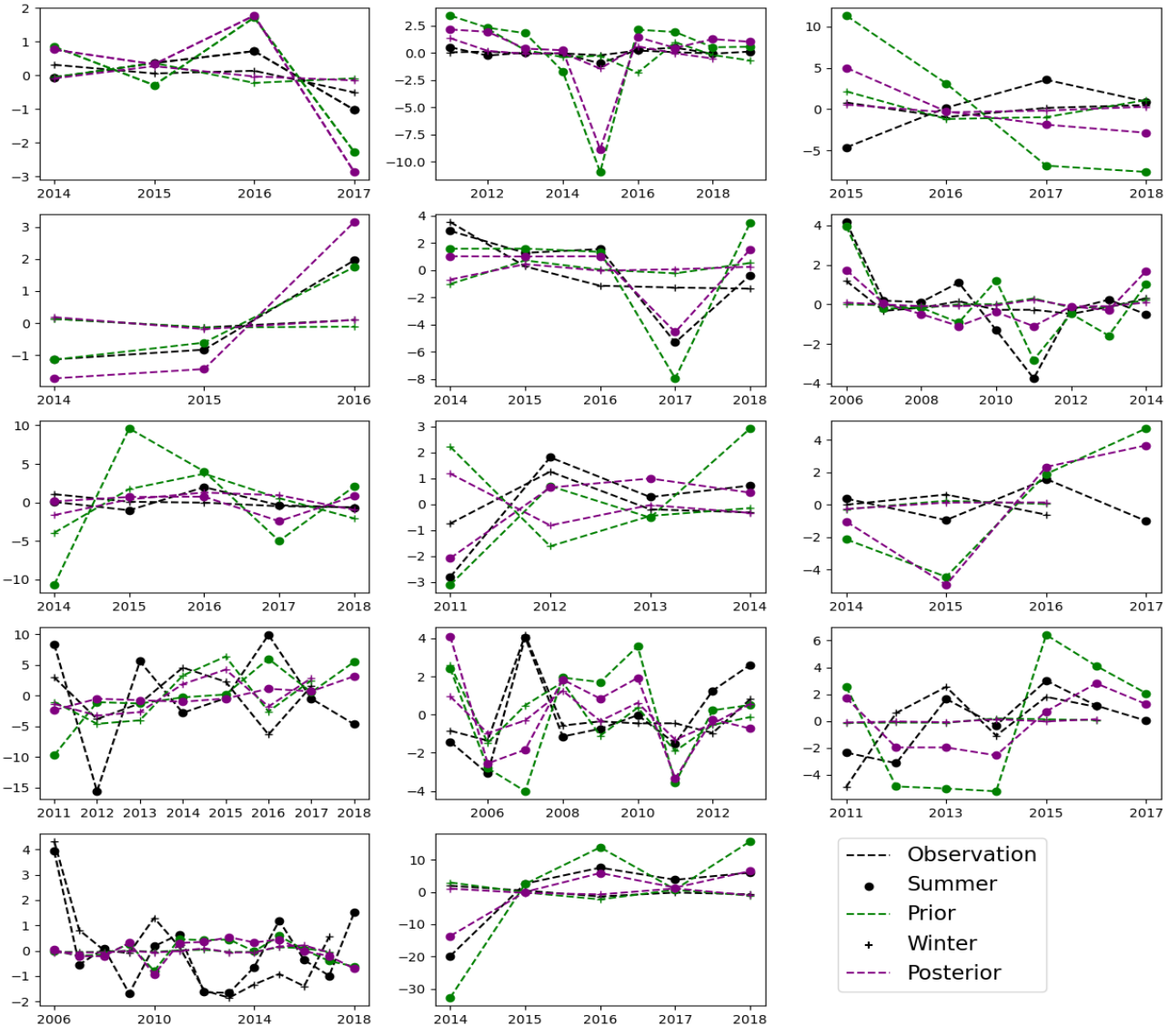

Figure B1. Summer and winter anomalies were estimated from the averages of the summer months (April to September) and winter months (October to March). The black, yellow, and purple dashed lines represent observations, prior, and posterior values, respectively. Dots and plus signs denote summer and winter data points of the season, respectively.

High deviations were observed in the summer anomaly compared to the winter anomaly at all the sites. In general, in the majority of cases, the model was capable enough to capture trends shown by the observational anomaly, though there were differences in magnitude. For example, for the sites Bon and Zak, the model was successful in capturing all the summer and

https://doi.org/10.5194/egusphere-2024-373
Preprint. Discussion started: 28 February 2024

winter trends of the observation. Notably, the high positive anomaly of Abi in 2016 and of Ole in 2015, etc., and the high negative anomaly of Att in 2015, of Deg in 2017, of Low in 2017, etc., were also captured by the model.

B2 The annual sum estimation of CH_4

The annual sum estimation of CH_4 from ten out of fourteen sites used in the study. Remaining four sites are illustrated and discussed in Sect. 3.4 of the paper. The figure illustrates that, after optimisation, most sites exhibited improved annual CH_4 estimation throughout the year. However, for the site Hue, the model consistently failed to capture the observation pattern in most years, and the site Att, particularly in the year 2016, also displayed shortcomings. On the other hand, Att in 2016 completely aligned with the observed value for both prior and posterior estimations.

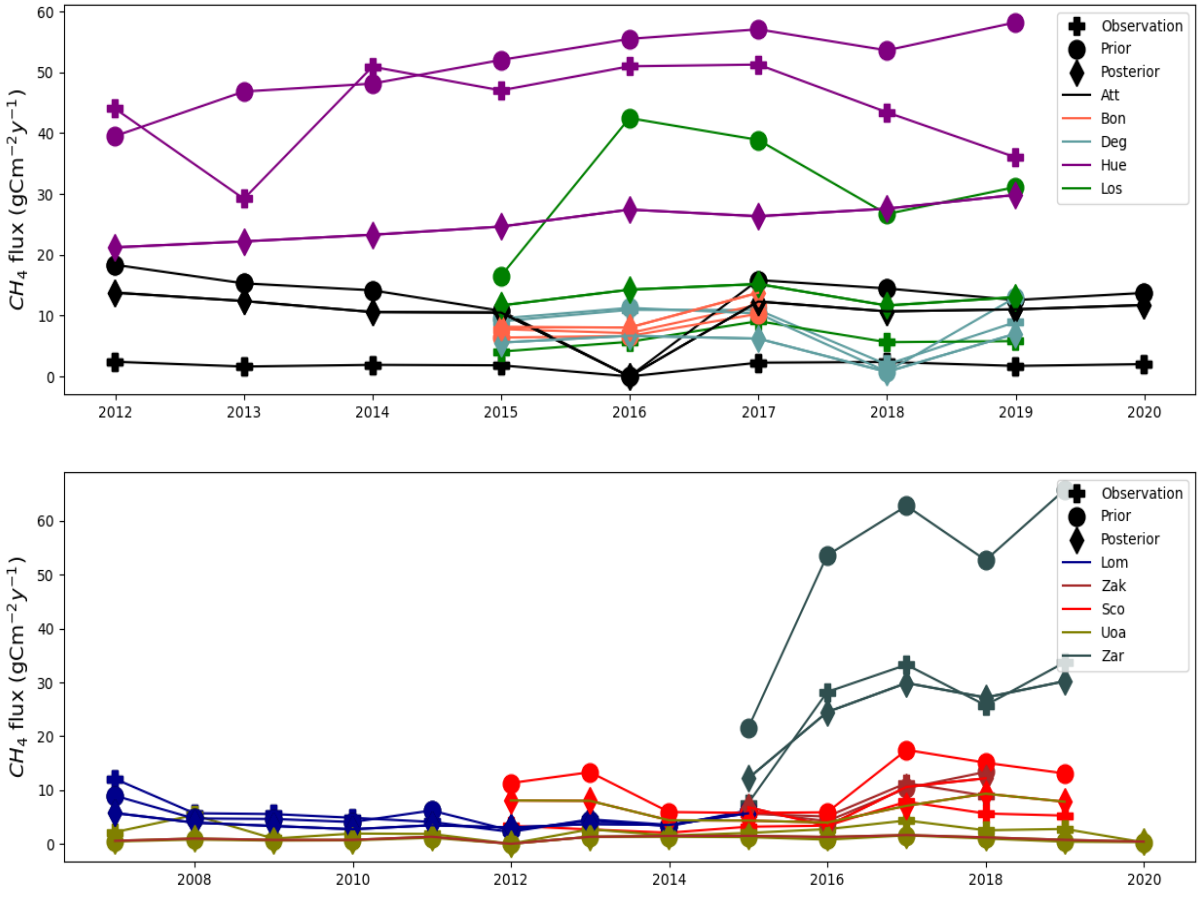

Figure B2. The annual sum estimation of CH_4 from ten out of 14 sites used in the study. The sites are represented in different colors with distinct markings to distinguish between Observation, Prior, and Posterior.

https://doi.org/10.5194/egusphere-2024-373
Preprint. Discussion started: 28 February 2024

Appendix C: Time series estimation of validation sites

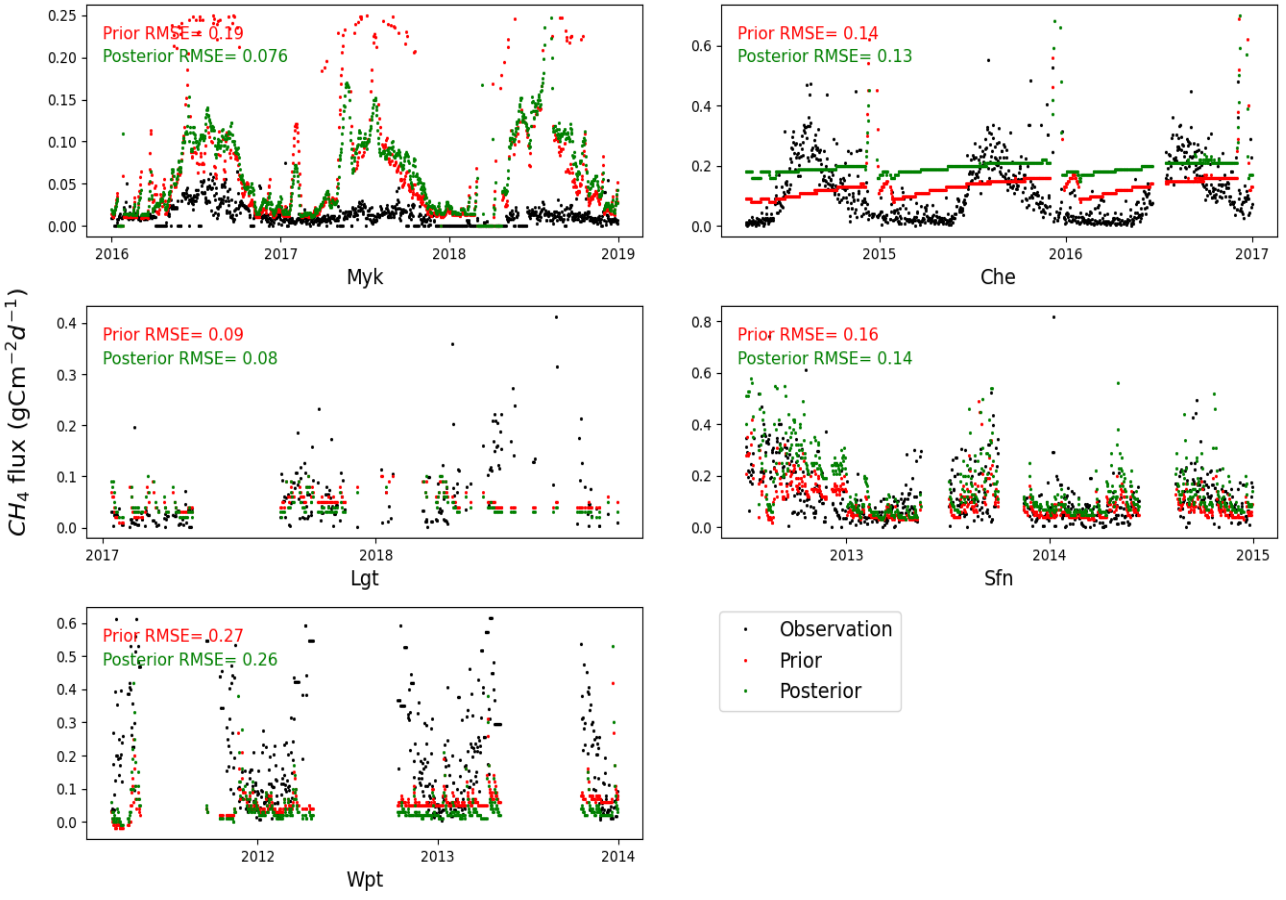

Figure C1. The CH_4 simulation from the LPJ-GUESS model is compared with observations from five different wetland sites used for validation. The black dots represent theCH_4 observations from corresponding wetlands. The red dots depict the prior simulation using the prior model parameters, while the green dots represent the posterior simulation with the posterior parameters. Three-day running averages are calculated from the original time series. In most of the figures, a few outliers on the vertical axis have been removed for better visualisation.

Author contributions. Conceptualisation was undertaken by JTK and MS. Methodology was formulated by JTK, JL, and MS. PM assisted in setting up the multi-site simulation in LPJ-GUESS. MA provided the CH_4 observations collected at Lompolojänkkä. PV and PW provided the observations collected at Mycklemossen. Setting up the GRaB-AM and writing the original draft was carried out by JTK. Editing were performed by JTK, MS, JL, PM, JR, PV, PW, and MA. All authors have read and agreed to the published version of the manuscript.

https://doi.org/10.5194/egusphere-2024-373
Preprint. Discussion started: 28 February 2024

Competing interests. The authors declare that they have no conflict of interest.

Acknowledgements. We would like to express our gratitude to Annalea Lohila, Kirsty Langley, Jutta Holst, and Elin Humphreys for their guidance on data repositories. Special thanks to Sadat Ismayil for assisting with computational resources. Additionally, we acknowledge the Fluxnet database, the Ameriflux database, the Integrated Carbon Observation System (ICOS), Greenland Ecosystem Monitoring (GEM), the Swedish Meteorological and Hydrological Institute (SMHI), the Swedish Infrastructure for Ecosystem Science (SITES), the Institute for Atmospheric and Earth System Research (SMEAR-INAR) at the University of Helsinki, and the Finnish Meteorological Institute (FMI) for providing open access to their data.

Financial support: This research has been supported by the Strategic Research Area: Biodiversity and Ecosystem services in a Changing Climate (BECC), Lund University, and is a contribution to the Strategic Research Area: ModElling the Regional and Global Earth system (MERGE). BECC and MERGE are funded by the Swedish government.

https://doi.org/10.5194/egusphere-2024-373
Preprint. Discussion started: 28 February 2024

References

Andrieu, C. and Thoms, J.: A tutorial on adaptive MCMC, Statistics and computing, 18, 343–373, 2008.

Aurela, M., Lohila, A., Tuovinen, J.-P., Hatakka, J., Penttilä, T., and Laurila, T.: Carbon dioxide and energy flux measurements in four northern-boreal ecosystems at Pallas, 2015.

Bohrer, G. and Morin, T. H.: FLUXNET-CH4 US-ORv Olentangy River Wetland Research Park, Tech. rep., FluxNet; The Ohio State Univ., Columbus, OH (United States), 2020.

Braswell, B. H., Sacks, W. J., Linder, E., and Schimel, D. S.: Estimating diurnal to annual ecosystem parameters by synthesis of a carbon flux model with eddy covariance net ecosystem exchange observations, Global Change Biology, 11, 335–355, 2005.

Canadell, J., Monteiro, P., Costa, M., da Cunha, L. C., Cox, P., Eliseev, A., Henson, S., Ishii, M., Jaccard, S., Koven, C., Lohila, A., Patra, P., Piao, S., Rogelj, J., Syampungani, S., Zaehle, S., and Zickfeld, K.: Global Carbon and other Biogeochemical Cycles and Feedbacks. In Climate Change 2021: The Physical Science Basis. Contribution of Working Group I to the Sixth Assessment Report of the Intergovernmental Panel on Climate Change, IPCC AR6 chapter 5, 2022.

Cao, M., Marshall, S., and Gregson, K.: Global carbon exchange and methane emissions from natural wetlands: Application of a process-based model, Journal of Geophysical Research: Atmospheres, 101, 14 399–14 414, 1996.

Chen, J. and Chu, H.: FLUXNET-CH4 US-CRT Curtice Walter-Berger cropland, Tech. rep., FluxNet; University of Toledo/Michigan State University, 2020.

Christensen, J. H., Hewitson, B., Busuioc, A., Chen, A., Gao, X., Held, I., Jones, R., Kolli, R. K., Kwon, W.-T., Laprise, R., et al.: Regional climate projections. Chapter 11, 2007.

Christensen, T. and Cox, P.: Response of methane emission from Arctic tundra to climatic change: results from a model simulation, Tellus B: Chemical and Physical Meteorology, 47, 301–309, 1995.

Delwiche, K. B., Knox, S. H., Malhotra, A., Fluet-Chouinard, E., McNicol, G., Feron, S., Ouyang, Z., Papale, D., Trotta, C., Canfora, E., et al.: FLUXNET-CH 4: a global, multi-ecosystem dataset and analysis of methane seasonality from freshwater wetlands, Earth system science data, 13, 3607–3689, 2021.

Desai, A. R. and Thom, J.: FLUXNET-CH4 US-Los Lost Creek, Tech. rep., FluxNet; Univ. of Wisconsin, Madison, WI (United States), 2020.

Desroziers, G., Berre, L., Chapnik, B., and Poli, P.: Diagnosis of observation, background and analysis-error statistics in observation space, Quarterly Journal of the Royal Meteorological Society: A journal of the atmospheric sciences, applied meteorology and physical oceanography, 131, 3385–3396, 2005.

Euskirchen, E. and Edgar, C.: FLUXNET-CH4 US-BZB Bonanza Creek Thermokarst Bog, Tech. rep., FluxNet, 2020.

Fick, S. E. and Hijmans, R. J.: WorldClim 2: new 1-km spatial resolution climate surfaces for global land areas, International journal of climatology, 37, 4302–4315, 2017.

Fung, I., John, J., Lerner, J., Matthews, E., Prather, M., Steele, L., and Fraser, P.: Three-dimensional model synthesis of the global methane cycle, Journal of Geophysical Research: Atmospheres, 96, 13 033–13 065, 1991.

Gedney, N., Cox, P., and Huntingford, C.: Climate feedback from wetland methane emissions, Geophysical Research Letters, 31, 2004.

Granberg, G., Sundh, I., Svensson, B., and Nilsson, M.: Effects of temperature, and nitrogen and sulfur deposition, on methane emission from a boreal mire, Ecology, 82, 1982–1998, 2001.

https://doi.org/10.5194/egusphere-2024-373
Preprint. Discussion started: 28 February 2024

Groenendijk, M., Dolman, A., Van der Molen, M., Leuning, R., Arneth, A., Delpierre, N., Gash, J., Lindroth, A., Richardson, A., Verbeeck, H., et al.: Assessing parameter variability in a photosynthesis model within and between plant functional types using global Fluxnet eddy covariance data, Agricultural and forest meteorology, 151, 22–38, 2011.

Iwata, H., Ueyama, M., and Harazono, Y.: FLUXNET-CH4 US-Uaf University of Alaska, Fairbanks, Tech. rep., FluxNet; Osaka Prefecture University; Shinshu University, 2020.

Jacotot, A., Gogo, S., and Laggoun-Défarge, F.: FLUXNET-CH4 FR-LGt La Guette, France, FLUXNET-CH4 Community Product [data set], 2020.

Kallingal, J. T., Lindström, J., Miller, P. A., Rinne, J., Raivonen, M., and Scholze, M.: Optimising CH 4 simulations from the LPJ-GUESS model v4. 1 using an adaptive MCMC algorithm, Geoscientific Model Development Discussions, 2023, 1–40, 2023.

Knorr, W. and Kattge, J.: Inversion of terrestrial ecosystem model parameter values against eddy covariance measurements by Monte Carlo sampling, Global change biology, 11, 1333–1351, 2005.

Koebsch, F. and Jurasinski, G.: FLUXNET-CH4 DE-Hte Huetelmoor, Tech. rep., FluxNet; Landscape Ecology, University of Rostock, 2020.

Kuppel, S., Peylin, P., Chevallier, F., Bacour, C., Maignan, F., and Richardson, A.: Constraining a global ecosystem model with multi-site eddy-covariance data, Biogeosciences, 9, 3757–3776, 2012.

Łakomiec, P., Holst, J., Friborg, T., Crill, P., Rakos, N., Kljun, N., Olsson, P.-O., Eklundh, L., Persson, A., and Rinne, J.: Field-scale CH 4 emission at a subarctic mire with heterogeneous permafrost thaw status, Biogeosciences, 18, 5811–5830, 2021.

Lasslop, G., Reichstein, M., Kattge, J., and Papale, D.: Influences of observation errors in eddy flux data on inverse model parameter estimation, Biogeosciences, 5, 1311–1324, 2008.

Lohila, A., Aurela, M., Tuovinen, J.-P., Laurila, T., Hatakka, J., Rainne, J., and Mäkelä, T.: FLUXNET-CH4 FI-Lom Lompolojankka, Tech. rep., FluxNet; Finnish Meteorological Institute, 2020.

McGuire, A., Sitch, S., Clein, J. S., Dargaville, R., Esser, G., Foley, J., Heimann, M., Joos, F., Kaplan, J., Kicklighter, D., et al.: Carbon balance of the terrestrial biosphere in the twentieth century: Analyses of CO2, climate and land use effects with four process-based ecosystem models, Global biogeochemical cycles, 15, 183–206, 2001.

Merbold, L., Fuchs, K., Buchmann, N., and Hörtnagl, L.: FLUXNET-CH4 CH-Cha Chamau, Tech. rep., FluxNet; ETH Zurich, 2020.

Monteil, G. and Scholze, M.: Regional CO 2 inversions with LUMIA, the Lund University modular inversion algorithm, v1. 0, Geoscientific Model Development, 14, 3383–3406, 2021.

Raoult, N. M., Jupp, T. E., Cox, P. M., and Luke, C. M.: Land-surface parameter optimisation using data assimilation techniques: the adJULES system V1. 0, Geoscientific Model Development, 9, 2833–2852, 2016.

Ringeval, B., de Noblet-Ducoudré, N., Ciais, P., Bousquet, P., Prigent, C., Papa, F., and Rossow, W. B.: An attempt to quantify the impact of changes in wetland extent on methane emissions on the seasonal and interannual time scales, Global Biogeochemical Cycles, 24, 2010.

Rinne, J., Tuittila, E.-S., Peltola, O., Li, X., Raivonen, M., Alekseychik, P., Haapanala, S., Pihlatie, M., Aurela, M., Mammarella, I., et al.: Temporal variation of ecosystem scale methane emission from a boreal fen in relation to temperature, water table position, and carbon dioxide fluxes, Global Biogeochemical Cycles, 32, 1087–1106, 2018.

Sachs, T., Wille, C., Larmanou, E., and Franz, D.: FLUXNET-CH4 DE-Zrk Zarnekow, Tech. rep., FluxNet; GFZ German Research Centre for Geosciences, 2020.

Saunois, M., Bousquet, P., Poulter, B., Peregon, A., Ciais, P., Canadell, J. G., Dlugokencky, E. J., Etiope, G., Bastviken, D., Houweling, S., et al.: The global methane budget 2000–2012, Earth System Science Data, 8, 697–751, 2016a.

https://doi.org/10.5194/egusphere-2024-373
Preprint. Discussion started: 28 February 2024

Saunois, M., Jackson, R., Bousquet, P., Poulter, B., and Canadell, J.: The growing role of methane in anthropogenic climate change, Environmental Research Letters, 11, 120 207, 2016b.

Saunois, M., Stavert, A. R., Poulter, B., Bousquet, P., Canadell, J. G., Jackson, R. B., Raymond, P. A., Dlugokencky, E. J., Houweling, S., Patra, P. K., et al.: The global methane budget 2000–2017, Earth system science data, 12, 1561–1623, 2020.

Scheller, J. H., Mastepanov, M., Christiansen, H. H., and Christensen, T. R.: Methane in Zackenberg Valley, NE Greenland: multidecadal growing season fluxes of a high-Arctic tundra, Biogeosciences, 18, 6093–6114, 2021.

Schmid, H. P. and Klatt, J.: FLUXNET-CH4 DE-SfN Schechenfilz Nord, Tech. rep., FluxNet; Karlsruhe Institute of Technology, Institute of Meteorology and . . . , 2020.

Segers, R. and Leffelaar, P. A.: Modeling methane fluxes in wetlands with gas-transporting plants: 3. Plot scale, Journal of Geophysical Research: Atmospheres, 106, 3541–3558, 2001.

Sitch, S., Smith, B., Prentice, I. C., Arneth, A., Bondeau, A., Cramer, W., Kaplan, J. O., Levis, S., Lucht, W., Sykes, M. T., et al.: Evaluation of ecosystem dynamics, plant geography and terrestrial carbon cycling in the LPJ dynamic global vegetation model, Global change biology, 9, 161–185, 2003.

Smith, B.: LPJ-GUESS-an ecosystem modelling framework, Department of Physical Geography and Ecosystems Analysis, INES, Sölvegatan, 12, 22 362, 2001.

Smith, B., Wårlind, D., Arneth, A., Hickler, T., Leadley, P., Siltberg, J., and Zaehle, S.: Implications of incorporating N cycling and N limitations on primary production in an individual-based dynamic vegetation model, Biogeosciences, 11, 2027–2054, 2014.

Sonnentag, O. and Helbig, M.: FLUXNET-CH4 CA-SCB Scotty Creek Bog, Tech. rep., FluxNet; Université de Montréal; Wilfrid Laurier University, 2020.

Susiluoto, J., Raivonen, M., Backman, L., Laine, M., Makela, J., Peltola, O., Vesala, T., and Aalto, T.: Calibrating the sqHIMMELI v1. 0 wetland methane emission model with hierarchical modeling and adaptive MCMC, Geoscientific Model Development, 11, 1199–1228, 2018.

Tarantola, A.: Inversion of travel times and seismic waveforms, Seismic tomography, pp. 135–157, 1987.

Todd, A. and Humphreys, E.: AmeriFlux AmeriFlux CA-ARF Attawapiskat River Fen, https://doi.org/10.17190/AMF/1480318, 2018.

Ueyama, M., Hirano, T., and Kominami, Y.: FLUXNET-CH4 JP-BBY Bibai bog, Tech. rep., FluxNet; Osaka Prefecture Univeristy, 2020.

University of East Anglia Climatic Research Unit (CRU), C. T. S. T. H. R. G. D.: Climatic Research Unit (CRU) time-series datasets of variations in climate with variations in other phenomena, 2006.

Walter, B. P. and Heimann, M.: A process-based, climate-sensitive model to derive methane emissions from natural wetlands: Application to five wetland sites, sensitivity to model parameters, and climate, Global Biogeochemical Cycles, 14, 745–765, 2000.

Wania, R., Ross, I., and Prentice, I.: Implementation and evaluation of a new methane model within a dynamic global vegetation model: LPJ-WHyMe v1. 3.1, Geoscientific Model Development, 3, 565–584, 2010.

White, J., Ahrén, D., Ström, L., Kelly, J., Klemedtsson, L., Keane, B., and Parmentier, F.: Methane Producing and Oxidizing Microorganisms Display a High Resilience to Drought in a Swedish Hemi-Boreal Mire, Journal of Geophysical Research: Biogeosciences, 128, e2022JG007 362, 2023.

Williams, M., Richardson, A. D., Reichstein, M., Stoy, P. C., Peylin, P., Verbeeck, H., Carvalhais, N., Jung, M., Hollinger, D. Y., Kattge, J., et al.: Improving land surface models with FLUXNET data, Biogeosciences, 6, 1341–1359, 2009.

Zhang, Z., Zimmermann, N. E., Stenke, A., Li, X., Hodson, E. L., Zhu, G., Huang, C., and Poulter, B.: Emerging role of wetland methane emissions in driving 21st century climate change, Proceedings of the National Academy of Sciences, 114, 9647–9652, 2017.

https://doi.org/10.5194/egusphere-2024-373
Preprint. Discussion started: 28 February 2024

Zhuang, Q., Melillo, J. M., Sarofim, M. C., Kicklighter, D. W., McGuire, A. D., Felzer, B. S., Sokolov, A., Prinn, R. G., Steudler, P. A., and Hu, S.: CO2 and CH4 exchanges between land ecosystems and the atmosphere in northern high latitudes over the 21st century, Geophysical Research Letters, 33, 2006.